Broadband Green's Function with Higher Order Low Wavenumber Extractions for an Inhomogeneous Waveguide with Irregular Shape

Tien-Hao Liao[1, *], Kung-Hau Ding[2], and Leung Tsang[3]

Abstract—The method of broadband Green's functions with low wavenumber extractions (BBGFL) is used to calculate Green's function for inhomogeneous waveguides filled with different dielectrics and with irregular boundaries. To construct the BBGFL modal solutions, we derive governing equations of the linear eigen-matrix problem and orthonormalization condition. In BBGFL, the Green's function is represented in modal expansions with convergence accelerated by higher order low wavenumber extractions. To obtain a linear eigenvalue problem for the modes, we use two BBGFLs of rectangular waveguides with two dielectric wavenumbers. The orthonormalized mode functions are used to construct the Green's function. Current wavenumber derivatives and Green's function wavenumber derivatives are computed by a single low wavenumber MoM impedance matrix. The wavenumber derivatives are used to accelerate the convergence of modal summations to 6th order. Numerical results are illustrated and compared with the direct MoM method of using free space Green's function. Results show accuracies and computation efficiencies for broadband simulations of Green's functions.

1. INTRODUCTION

Green's function is a fundamental concept in electromagnetics and is the system response due to a point source [1–5]. In computational electromagnetics (CEM), the free space Green's function is frequently used. The free space Green's functions do not satisfy boundary conditions. They are used to formulate integral equations that satisfy boundary conditions. The integral equations are then solved to calculate scattering solutions. We label this method as the "scattering method". The scattering method needs to be repeated whenever the frequency is changed which hinders its usage in broadband modeling and simulations. Hence, it is useful to develop fast techniques for computing the Green's function.

For the waveguide problem, the Boundary Integral-Resonant Mode Expansion (BIRME) method with DC extractions was used to compute the modes of an arbitrary shaped homogeneous waveguides [6–8]. Recently, we have developed a methodology which is called the Broadband Green's Functions with Low wavenumber extractions (BBGFL). We used the BBGFL method to calculate the Green's function over a broad frequency range for homogeneous waveguides with irregular geometries [9–15]. The BBGFL method has also been applied to periodic structures [16–19]. In the BBGFL approach, we compute the modal field solutions which satisfy the waveguide boundary conditions and thus contain all the multiple scattering solutions. The broad band Green's functions are expressed in terms of the computed modal solutions. The solution of the Green's function at every frequency is obtained by merely changing the denominator in the modal summation expression.

There are four one-time set-up steps required in the BBGFL technique. (i) The modal field solutions, eigenvalues, and eigenvectors are cast in a linear eigenvalue problem of relative small size so that the eigenvalues and eigenvectors are solved simultaneously. (ii) The modal field solutions are in a hybrid representation with a boundary integral part and a modal expansion part. The hybrid representation give accurate field solutions. (iii) The normalizations of the modal field solutions are

* Corresponding author: Tien-Hao Liao (tien-hao.liao@jpl.nasa.gov).
[1] California Institute of Technology, USA. [2] Air Force Research Laboratory, USA. [3] University of Michigan, USA.

performed efficiently without requiring volumetric integration, and (iv) The low wavenumber extraction is exercised to accelerate the convergence of modal summation. Using wavenumber derivative, we have achieved a 6th order convergence for BBGFL [15]. Note that the 4 set-up steps are only performed once and the BBGFL Green's function is applicable for all frequencies by merely changing the denominator.

In this paper we use the BBGFL method for the problem of an inhomogeneous waveguide filled with two different dielectrics. In classical waveguide problems, homogeneous waveguides of separable geometry were solved extensively. However, inhomogeneous waveguides are seldom addressed and analytical solutions are generally not possible. For BBGFL, the extension from homogeneous waveguide to inhomogeneous is not trivial. The introduction of interface between different dielectrics results in coupled formulation of integral equations and solutions are much more complicated than the homogeneous case. Other complexities are in deriving the linear eigenvalue problem for the solutions of mode wavenumbers and normalized modal fields for an inhomogeneous waveguide with irregular shape. In the set-up steps, we use two rectangular waveguide Green's functions with different dielectric constants to derive the linear eigen-matrix equation. The integral equation on the dielectric interface couples two different Green's functions. The mode field solution is in a linear combination of boundary integrals and the mode summations. For inhomogeneous waveguide mode normalization, we derive new orthonormality condition that do require volumetric integrations. To accelerate the convergence of modal summation, we develop the wavenumber derivative technique to achieve the 6th order convergence.

This paper is organized as follows. In Section 2, the modal eigenvalues and field solutions and the ortho-normalization of modes are derived. We also describe the method of spurious mode rejection. In Section 3, we derive wavenumber derivatives for currents and Green's functions to accelerate convergence of modal convergence. In Section 4, Numerical results are illustrated. Comparisons are made with results from direct MoM method and from HFSS. Conclusions are given in Section 5.

2. MODAL SOLUTIONS OF INHOMOGENEOUS WAVEGUIDE WITH IRREGULAR SHAPE

An irregularly shaped waveguide S with Dirichlet boundary conditions is shown in Figure 1. The waveguide is divided into two regions A_1 and A_2 with respective dielectrics, ε_1 and ε_2. The two regions
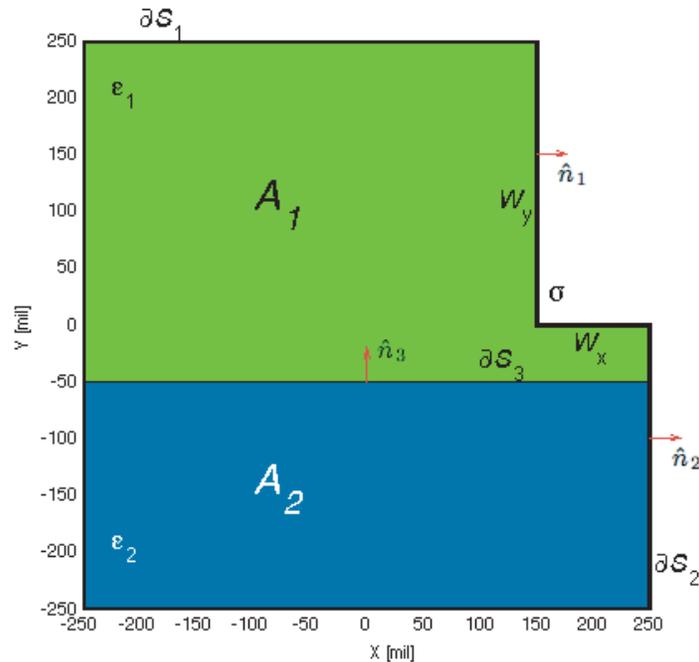
Figure 1. Irregular shaped inhomogeneous waveguide with Dirichlet boundary condition. Two dielectrics are ε_1 and ε_2.

are separated by the interface ∂S_3. The boundaries for regions A_1 and A_2 are denoted by ∂S_1 and ∂S_2, respectively. The boundary of waveguide S is $\partial S = \partial S_1 + \partial S_2$. The irregular part of ∂S is denoted by σ. The normal unit vectors $\hat{n}_1$, $\hat{n}_2$, and $\hat{n}_3$ are shown for the respective boundaries ∂S_1, ∂S_2, and ∂S_3. There are four one-time set-up steps required in the BBGFL technique.

2.1. Linear Eigen-Value Problem for Modal Solutions

The step 1 of setup is to derive a linear eigenvalue problem for modal solutions. The modal fields $\psi^S(\bar{\rho})$ are expressed as

$$\psi^S(\bar{\rho}) = \begin{cases} \psi_1^S(\bar{\rho}) & \text{for } \bar{\rho} \text{ in } A_1 \\ \psi_2^S(\bar{\rho}) & \text{for } \bar{\rho} \text{ in } A_2 \end{cases} \tag{1}$$

where ψ_1^S and ψ_2^S obey the following wave equation (1) and boundary conditions (2) and (3).

$$\nabla_t^2 \psi_\xi^S(\bar{\rho}) + k_\xi^2 \psi_\xi^S(\bar{\rho}) = 0 \tag{2}$$

$$\begin{aligned} \psi_1^S(\bar{\rho}) &= \psi_2^S(\bar{\rho}) & \bar{\rho} \text{ on } \partial S_3 \\ \frac{\partial \psi_1^S(\bar{\rho})}{\partial n} &= \frac{\partial \psi_2^S(\bar{\rho})}{\partial n} & \bar{\rho} \text{ on } \partial S_3 \\ \psi_\xi^S(\bar{\rho}) &= 0 & \bar{\rho} \text{ on } \partial S_{1,2} \end{aligned} \tag{3}$$

where $\xi = 1, 2$ and $k_2^2 = \frac{\varepsilon_2}{\varepsilon_1} k_1^2$.

To obtain a linear eigenvalue problem, we use two Green's functions $g^\Omega(k_1, \bar{\rho}, \bar{\rho}')$ and $g^\Omega(k_2, \bar{\rho}, \bar{\rho}')$ of the rectangular waveguide Ω with wavenumber k_1 and k_2, respectively. Eq. (4) is the modal function for the rectangular waveguide of size L_x by L_y.

$$\psi_\alpha^\Omega(\bar{\rho}) = \frac{2}{\sqrt{L_x L_y}} \sin\left(\frac{p\pi}{L_x}\left(x + \frac{L_x}{2}\right)\right) \sin\left(\frac{q\pi}{L_y}\left(y + \frac{L_y}{2}\right)\right) \tag{4}$$

where, p and q are modal index in x- and y-direction, and α is a combined mode index for the rectangle waveguide Ω. By extracting a low wavenumber $k_{\xi L}^\Omega$, Green's function $g^\Omega(k_\xi, \bar{\rho}, \bar{\rho}')$ is expressed as

$$g^\Omega(k_\xi, \bar{\rho}, \bar{\rho}') = g^\Omega(k_{\xi L}^\Omega, \bar{\rho}, \bar{\rho}') + \sum_\alpha \frac{\left[k_\xi^2 - \left(k_{\xi L}^\Omega\right)^2\right] \psi_\alpha^\Omega(\bar{\rho}) \psi_\alpha^\Omega(\bar{\rho}')}{\left[(k_\alpha^\Omega)^2 - k_\xi^2\right]\left[(k_\alpha^\Omega)^2 - \left(k_{\xi L}^\Omega\right)^2\right]} \tag{5}$$

where $\xi = 1, 2$. Note that $g^\Omega(k_\xi, \bar{\rho}, \bar{\rho}')$ is separated into a low wavenumber part and a broad band part.

Next, we apply Green's theorems in regions A_1 and A_2 to construct the integral Eqs. (6) and (7), respectively.

$$\int_\sigma \left[-g^\Omega(k_1, \bar{\rho}, \bar{\rho}') \hat{n}_1' \cdot \nabla_t' \psi_1^S(\bar{\rho}')\right] dl' + \int_{\partial S_3} \psi_1^S(\bar{\rho}')(-\hat{n}_3') \cdot \nabla_t' g^\Omega(k_1, \bar{\rho}, \bar{\rho}') dl'$$

$$- \int_{\partial S_3} g^\Omega(k_1, \bar{\rho}, \bar{\rho}')(-\hat{n}_3') \cdot \nabla_t' \psi_1^S(\bar{\rho}') dl' = 0 \tag{6}$$

$$\int_{\partial S_3} \psi_2^S(\bar{\rho}') \hat{n}_3' \cdot \nabla_t' g^\Omega(k_2, \bar{\rho}, \bar{\rho}') dl' - \int_{\partial S_3} g^\Omega(k_2, \bar{\rho}, \bar{\rho}') \hat{n}_3' \cdot \nabla_t' \psi_2^S(\bar{\rho}') dl' = 0 \tag{7}$$

Note that the integral equations are not on the entire boundary but only on the boundaries σ and ∂S_3. The rectangular waveguide Green's functions in Eq. (5) are substituted into Eqs. (6) and (7). Solutions are calculated by using MoM with pulse basis functions and point matching. We used small values of $k_{\xi L}^\Omega$ for convergence of modal expansions and to facilitate mode normalizations. In addition, a higher order integration quadrature is applied to compute the low wavenumber MoM solutions of $g^\Omega(k_{\xi L}^\Omega, \bar{\rho}, \bar{\rho}')$ accurately. The low wavenumber Green's functions are computed once only. Let $\bar{\rho}_n$ be the center of

the n-th patch and Δt_n be the patch length. As shown in Eq. (8), the surface unknowns are fields on interface ∂S_3, x_n, the normal derivatives of fields on interface ∂S_3, y_n, and the normal derivatives of fields on boundary σ, z_n.

$$x_n = \Delta t_n^{\partial S_3} \psi^S \left(\bar{\rho}_n^{\partial S_3} \right) \qquad\qquad n = 1, 2, \ldots, N_3$$

$$y_n = \Delta t_n^{\partial S_3} \left[\hat{n}_3' \cdot \nabla_t' \psi^S \left(\bar{\rho}' \right) \right]_{\bar{\rho}' = \bar{\rho}_n^{\partial S_3}} \qquad n = 1, 2, \ldots, N_3 \qquad (8)$$

$$z_n = \Delta t_n^{\sigma} \left[\hat{n}_1' \cdot \nabla_t' \psi^S \left(\bar{\rho}' \right) \right]_{\bar{\rho}' = \bar{\rho}_n^{\sigma}} \qquad n = 1, 2, \ldots, N_0$$

where N_3 is the number of patches on ∂S_3, and N_0 is the number of patches on σ.

There are a total of five integrals in Eqs. (6) and (7). In the following, we describe the evaluation of the second integral of Eq. (6). Let β be the modal index of waveguide S and $k_1 = k_{1\beta}$. The surface integral is tested at $\bar{\rho}_m^{\partial S_3}$ which is in medium 1 and close to ∂S_3. Then we have

$$\int_{\partial S_3} \left[\psi_\beta^S \left(\bar{\rho}' \right) \hat{n}_3' \cdot \nabla_t' g^\Omega \left(k_{1\beta}^S, \bar{\rho}_m^{\partial S_3}, \bar{\rho}' \right) \right] dl' = \sum_n A_{3mn}^{(1)L} x_{\beta n} + \sum_\alpha R_{3m\alpha}^{(1)L} a_{\beta\alpha}^{(1)L} \qquad (9)$$

where

$$A_{3mn}^{(1)L} = \frac{1}{\Delta t_n^{\partial S_3}} \int_{\partial S_3^{(n)}} \hat{n}_3' \cdot \nabla_t' g^\Omega \left(k_{1L}^\Omega, \bar{\rho}_m^{\partial S_3}, \bar{\rho}' \right) dl' \qquad (10)$$

$$a_{\beta\alpha}^{(1)L} = \frac{\left(k_{1\beta}^S \right)^2 - \left(k_{1L}^\Omega \right)^2}{\left(k_\alpha^\Omega \right)^2 - \left(k_{1\beta}^S \right)^2} \int_{\partial S_3} \psi_\beta^S \left(\bar{\rho}' \right) \hat{n}_3' \cdot \nabla_t' \psi_\alpha^\Omega \left(\bar{\rho}' \right) dl' \qquad (11)$$

$$R_{3m\alpha}^{(1)L} = \frac{\psi_\alpha^\Omega \left(\bar{\rho}_m^{\partial S_3} \right)}{\left(k_\alpha^\Omega \right)^2 - \left(k_{1L}^\Omega \right)^2} \qquad (12)$$

The superscript L in Eqs. (10)–(12) denotes the low wavenumber and the superscript (1) for the observation in medium 1. On the right-hand side of Eq. (9), the low wavenumber part of g^Ω gives the first term, and the second term results from the modal contribution of ψ_α^Ω. The modal coefficient $a_{\beta\alpha}^{(1)L}$ shows the coupling between the waveguide modes of ψ_β^S and ψ_α^Ω. Similar procedures are then applied to the other two integrals in Eq. (6) with testing points in medium 1 and very close to ∂S_3. Expressions for the corresponding matrix elements are shown in Eqs. (13)–(16).

$$B_{3mn}^{(1)L} = \frac{1}{\Delta t_n^{\partial S_3}} \int_{\partial S_3^{(n)}} g^\Omega \left(k_{1L}^\Omega, \bar{\rho}_m^{\partial S_3}, \bar{\rho}' \right) dl' \qquad (13)$$

$$C_{3mn}^{(1)L} = \frac{1}{\Delta t_n^\sigma} \int_{\sigma^{(n)}} g^\Omega \left(k_{1L}^\Omega, \bar{\rho}_m^{\partial S_3}, \bar{\rho}' \right) dl' \qquad (14)$$

$$b_{\beta\alpha}^{(1)L} = \frac{\left(k_{1\beta}^S \right)^2 - \left(k_{1L}^\Omega \right)^2}{\left(k_\alpha^\Omega \right)^2 - \left(k_{1\beta}^S \right)^2} \int_{\partial S_3} \psi_\alpha^\Omega \left(\bar{\rho}' \right) \hat{n}_3' \cdot \nabla_t' \psi_\beta^S \left(\bar{\rho}' \right) dl' \qquad (15)$$

$$c_{\beta\alpha}^{(1)L} = \frac{\left(k_{1\beta}^S \right)^2 - \left(k_{1L}^\Omega \right)^2}{\left(k_\alpha^\Omega \right)^2 - \left(k_{1\beta}^S \right)^2} \int_\sigma \psi_\alpha^\Omega \left(\bar{\rho}' \right) \hat{n}_1' \cdot \nabla_t' \psi_\beta^S \left(\bar{\rho}' \right) dl' \qquad (16)$$

Similarly, modal coefficients $b_{\beta\alpha}^{(1)L}$ and $c_{\beta\alpha}^{(1)L}$ show the coupling between the waveguide modes of ψ_β^S and ψ_α^Ω. Next, we test Eq. (7) with points very close to ∂S_3 in medium 2. Eqs. (17)–(21) are the corresponding matrix elements.

$$A_{3mn}^{(2)L} = \frac{1}{\Delta t_n^{\partial S_3}} \int_{\partial S_3^{(n)}} \hat{n}_3' \cdot \nabla_t' g^\Omega \left(k_{2L}^\Omega, \bar{\rho}_m^{\partial S_3}, \bar{\rho}' \right) dl' \qquad (17)$$

$$B_{3mn}^{(2)L} = \frac{1}{\Delta t_n^{\partial S_3}} \int_{\partial S_3^{(n)}} g^{\Omega} \left(k_{2L}^{\Omega}, \bar{\rho}_m^{\partial S_3}, \bar{\rho}' \right) dl' \tag{18}$$

$$R_{3m\alpha}^{(2)L} = \frac{\psi_{\alpha}^{\Omega} \left(\bar{\rho}_m^{\partial S_3} \right)}{\left(k_{\alpha}^{\Omega} \right)^2 - \left(k_{2L}^{\Omega} \right)^2} \tag{19}$$

$$a_{\beta\alpha}^{(2)L} = \frac{\left(k_{2\beta}^{S} \right)^2 - \left(k_{2L}^{\Omega} \right)^2}{\left(k_{\alpha}^{\Omega} \right)^2 - \left(k_{2\beta}^{S} \right)^2} \int_{\partial S_3} \psi_{\beta}^{S} \left(\bar{\rho}' \right) \hat{n}_3' \cdot \nabla_t' \psi_{\alpha}^{\Omega} \left(\bar{\rho}' \right) dl' \tag{20}$$

$$b_{\beta\alpha}^{(2)L} = \frac{\left(k_{2\beta}^{S} \right)^2 - \left(k_{2L}^{\Omega} \right)^2}{\left(k_{\alpha}^{\Omega} \right)^2 - \left(k_{2\beta}^{S} \right)^2} \int_{\partial S_3} \psi_{\alpha}^{\Omega} \left(\bar{\rho}' \right) \hat{n}_3' \cdot \nabla_t' \psi_{\beta}^{S} \left(\bar{\rho}' \right) dl' \tag{21}$$

Last, we test Eq. (7) with points very close to σ in medium 1. Eqs. (22)–(25) are the corresponding matrix components.

$$A_{0mn}^{(1)L} = \frac{1}{\Delta t_n^{\partial S_3}} \int_{\partial S_3^{(n)}} \hat{n}_3' \cdot \nabla_t' g^{\Omega} \left(k_{1L}^{\Omega}, \bar{\rho}_m^{\sigma}, \bar{\rho}' \right) dl' \tag{22}$$

$$B_{0mn}^{(1)L} = \frac{1}{\Delta t_n^{\partial S_3}} \int_{\partial S_3^{(n)}} g^{\Omega} \left(k_{1L}^{\Omega}, \bar{\rho}_m^{\sigma}, \bar{\rho}' \right) dl' \tag{23}$$

$$C_{0mn}^{(1)L} = \frac{1}{\Delta t_n^{\sigma}} \int_{\partial S_3^{(n)}} g^{\Omega} \left(k_{1L}^{\Omega}, \bar{\rho}_m^{\sigma}, \bar{\rho}' \right) dl' \tag{24}$$

$$R_{0m\alpha}^{(1)L} = \frac{\psi_{\alpha}^{\Omega} \left(\bar{\rho}_m^{\sigma} \right)}{\left(k_{\alpha}^{\Omega} \right)^2 - \left(k_{1L}^{\Omega} \right)^2} \tag{25}$$

From Eqs. (10)–(25), we derive the coupled matrix equations in Eqs. (26)–(28).

$$\overline{\overline{A}}_3^{(1)L} \bar{x}_{\beta} - \overline{\overline{B}}_3^{(1)L} \bar{y}_{\beta} - \overline{\overline{C}}_3^{(1)L} \bar{z}_{\beta} = -\overline{\overline{R}}_3^{(1)L} \bar{a}_{\beta}^{(1)L} + \overline{\overline{R}}_3^{(1)L} \bar{b}_{\beta}^{(1)L} + \overline{\overline{R}}_3^{(1)L} \bar{c}_{\beta}^{(1)L} \tag{26}$$

$$\overline{\overline{A}}_3^{(2)L} \bar{x}_{\beta} - \overline{\overline{B}}_3^{(2)L} \bar{y}_{\beta} = -\overline{\overline{R}}_3^{(2)L} \bar{a}_{\beta}^{(2)L} + \overline{\overline{R}}_3^{(2)L} \bar{b}_{\beta}^{(2)L} \tag{27}$$

$$\overline{\overline{A}}_0^{(1)L} \bar{x}_{\beta} - \overline{\overline{B}}_0^{(1)L} \bar{y}_{\beta} - \overline{\overline{C}}_0^{(1)L} \bar{z}_{\beta} = -\overline{\overline{R}}_0^{(1)L} \bar{a}_{\beta}^{(1)L} + \overline{\overline{R}}_0^{(1)L} \bar{b}_{\beta}^{(1)L} + \overline{\overline{R}}_0^{(1)L} \bar{c}_{\beta}^{(1)L} \tag{28}$$

where we have put the surface unknowns, $\bar{x}_{\beta}$, $\bar{y}_{\beta}$, and $\bar{z}_{\beta}$, on the left-hand side and the modal coefficients, $\bar{a}_{\beta}^{(1)L}$, $\bar{b}_{\beta}^{(1)L}$, $\bar{c}_{\beta}^{(1)L}$, $\bar{a}_{\beta}^{(2)L}$, and $\bar{b}_{\beta}^{(2)L}$ on the right-hand side. The indices in the superscript denote the regions where the surface integrals are calculated. Let

$$\bar{J}_{\beta}^{L} = \left[\begin{array}{ccc} \bar{x}_{\beta}^{T} & \bar{y}_{\beta}^{T} & \bar{z}_{\beta}^{T} \end{array} \right]^{T} \tag{29}$$

and

$$\bar{v}_{\beta}^{L} = \left[\begin{array}{ccccc} \left[\bar{a}_{\beta}^{(1)L} \right]^{T} & \left[\bar{a}_{\beta}^{(2)L} \right]^{T} & \left[\bar{b}_{\beta}^{(1)L} \right]^{T} & \left[\bar{b}_{\beta}^{(2)L} \right]^{T} & \left[\bar{c}_{\beta}^{(1)L} \right]^{T} \end{array} \right]^{T} \tag{30}$$

we form a matrix equation from Eqs. (26)–(28).

$$\bar{J}_{\beta}^{L} = \overline{\overline{M}}^{L} \bar{v}_{\beta}^{L} \tag{31}$$

where

$$\overline{\overline{M}}^{L} = \left[\begin{array}{ccc} \overline{\overline{A}}_3^{(1)L} & -\overline{\overline{B}}_3^{(1)L} & -\overline{\overline{C}}_3^{(1)L} \\ \overline{\overline{A}}_3^{(2)L} & -\overline{\overline{B}}_3^{(2)L} & \overline{\overline{0}} \\ \overline{\overline{A}}_0^{(1)L} & -\overline{\overline{B}}_0^{(1)L} & -\overline{\overline{C}}_0^{(1)L} \end{array} \right]^{-1} \left[\begin{array}{ccccc} -\overline{\overline{R}}_3^{(1)L} & \overline{\overline{0}} & \overline{\overline{R}}_3^{(1)L} & \overline{\overline{0}} & \overline{\overline{R}}_3^{(1)L} \\ \overline{\overline{0}} & -\overline{\overline{R}}_3^{(2)L} & \overline{\overline{0}} & \overline{\overline{R}}_3^{(2)L} & \overline{\overline{0}} \\ -\overline{\overline{R}}_0^{(1)L} & \overline{\overline{0}} & \overline{\overline{R}}_0^{(1)L} & \overline{\overline{0}} & \overline{\overline{R}}_0^{(1)L} \end{array} \right] \tag{32}$$

In Eq. (31), $\overline{\overline{M}}^L$ links the boundary unknowns in terms of modal coefficients.

Next, we proceed to derive a linear eigenvalue matrix equation for the modal coefficients by expressing surface unknowns in terms of modal coefficients, $\bar{a}_\beta^{(1)L}$, $\bar{b}_\beta^{(1)L}$, $\bar{c}_\beta^{(1)L}$, $\bar{a}_\beta^{(2)L}$, and $\bar{b}_\beta^{(2)L}$. For the modal coefficient $a_{\beta\alpha}^{(1)L}$, after some algebraic manipulations, we obtain the following equation with resonant wavenumber on the right-hand side.

$$D_{\alpha\alpha}^{(1)L} a_{\beta\alpha}^{(1)L} + \sum_n Q_{3n\alpha}^{(1)L} x_{\beta n} = E_{\beta\beta}^{(1)L} a_{\beta\alpha}^{(1)L} \tag{33}$$

where

$$Q_{3n\alpha}^{(1)L} = \frac{\left[\hat{n}_3' \cdot \nabla_t' \psi_\alpha^\Omega(\vec{\rho}')\right]_{\vec{\rho}'=\vec{\rho}_n^{\partial S_3}}}{(k_\alpha^\Omega)^2 - (k_{1L}^\Omega)^2} \tag{34}$$

$$D_{\alpha\alpha}^{(1)L} = \frac{1}{(k_\alpha^\Omega)^2 - (k_{1L}^\Omega)^2} \tag{35}$$

$$E_{\beta\beta}^{(1)L} = \frac{1}{\left(k_{1\beta}^S\right)^2 - (k_{1L}^\Omega)^2} \tag{36}$$

We note that $Q_{3n\alpha}^{(1)L}$ only depends on the rectangular waveguide modes while $D_{\alpha\alpha}^{(1)L}$ and $E_{\beta\beta}^{(1)L}$ are elements of diagonal matrices. In the matrix form, Eq. (33) is written as

$$\overline{\overline{D}}^{(1)L} \bar{a}_\beta^{(1)L} + \left[\overline{\overline{Q}}_3^{(1)L}\right]^T \bar{x}_\beta = \overline{\overline{E}}_\beta^{(1)L} \bar{a}_\beta^{(1)L} \tag{37}$$

Similar procedures are further applied to the other four modal coefficients. We obtain the matrix equation (38).

$$\overline{\overline{D}}^L \bar{v}_\beta^L + \left[\overline{\overline{Q}}^L\right]^T \bar{J}_\beta^L = \overline{\overline{E}}^L \bar{v}_\beta^L \tag{38}$$

where

$$\overline{\overline{D}}^L = \begin{bmatrix} \overline{\overline{D}}^{(1)L} & \overline{\overline{0}} & \overline{\overline{0}} & \overline{\overline{0}} & \overline{\overline{0}} \\ \overline{\overline{0}} & \frac{\varepsilon_2}{\varepsilon_1}\overline{\overline{D}}^{(2)L} & \overline{\overline{0}} & \overline{\overline{0}} & \overline{\overline{0}} \\ \overline{\overline{0}} & \overline{\overline{0}} & \overline{\overline{D}}^{(1)L} & \overline{\overline{0}} & \overline{\overline{0}} \\ \overline{\overline{0}} & \overline{\overline{0}} & \overline{\overline{0}} & \frac{\varepsilon_2}{\varepsilon_1}\overline{\overline{D}}^{(2)L} & \overline{\overline{0}} \\ \overline{\overline{0}} & \overline{\overline{0}} & \overline{\overline{0}} & \overline{\overline{0}} & \overline{\overline{D}}^{(1)L} \end{bmatrix} \tag{39}$$

$$\left[\overline{\overline{Q}}^L\right]^T = \begin{bmatrix} \left[\overline{\overline{Q}}_3^{(1)L}\right]^T & \overline{\overline{0}} & \overline{\overline{0}} \\ \frac{\varepsilon_2}{\varepsilon_1}\left[\overline{\overline{Q}}_3^{(2)L}\right]^T & \overline{\overline{0}} & \overline{\overline{0}} \\ \overline{\overline{0}} & \left[\overline{\overline{R}}_3^{(1)L}\right]^T & \overline{\overline{0}} \\ \overline{\overline{0}} & \frac{\varepsilon_2}{\varepsilon_1}\left[\overline{\overline{R}}_3^{(2)L}\right]^T & \overline{\overline{0}} \\ \overline{\overline{0}} & \overline{\overline{0}} & \left[\overline{\overline{R}}_0^{(1)L}\right]^T \end{bmatrix} \tag{40}$$

$$\overline{\overline{E}}^L = \begin{bmatrix} \overline{\overline{E}}^{(1)L} & \overline{\overline{0}} & \overline{\overline{0}} & \overline{\overline{0}} & \overline{\overline{0}} \\ \overline{\overline{0}} & \overline{\overline{E}}^{(1)L} & \overline{\overline{0}} & \overline{\overline{0}} & \overline{\overline{0}} \\ \overline{\overline{0}} & \overline{\overline{0}} & \overline{\overline{E}}^{(1)L} & \overline{\overline{0}} & \overline{\overline{0}} \\ \overline{\overline{0}} & \overline{\overline{0}} & \overline{\overline{0}} & \overline{\overline{E}}^{(1)L} & \overline{\overline{0}} \\ \overline{\overline{0}} & \overline{\overline{0}} & \overline{\overline{0}} & \overline{\overline{0}} & \overline{\overline{E}}^{(1)L} \end{bmatrix} \tag{41}$$

Substituting Eq. (31) into Eq. (38) yields the linear eigenvalue matrix equation.

$$\overline{\overline{P}}^L \bar{v}^L_\beta = \lambda^L_\beta \bar{v}^L_\beta \tag{42}$$

where

$$\overline{\overline{P}}^L = \overline{\overline{D}}^L + \left[\overline{\overline{Q}}^L\right]^T \overline{\overline{M}}^L \tag{43}$$

and the eigen-value λ^L_β is related to the corresponding mode wavenumber $k^S_{1\beta}$.

$$k^S_{1\beta} = \sqrt{\left(k^\Omega_{1L}\right)^2 + \frac{1}{\lambda^L_\beta}} \tag{44}$$

Note that the above is a linear eigenvalue problem because the matrices are independent of the eigenvalues. $\overline{\overline{P}}^L$ depends only on the low wavenumber k^Ω_{1L} and waveguide Ω modes. On the other hand, if the usual free space Green's function is used with MoM, the eigenvalue problem becomes nonlinear as the matrices depend on the eigenvalues. Nonlinear eigenvalue problems require calculating the matrix elements for each iteration of the search.

2.2. Hybrid Representation of Modal Field Solutions

The modal functions, $\psi^S_{1\beta}(\bar\rho)$ and $\psi^S_{2\beta}(\bar\rho)$, in regions 1 and 2, are derived using Green's theorems again in regions A_1 and A_2.

$$\int_{\partial S_3} \psi^S_\beta(\bar\rho')\hat{n}'_3 \cdot \nabla'_t g^\Omega\left(k^\Omega_{1L}, \bar\rho, \bar\rho'\right) dl' - \int_{\partial S_3} g^\Omega\left(k^\Omega_{1L}, \bar\rho, \bar\rho'\right)\hat{n}'_3 \cdot \nabla'_t\psi^S_\beta(\bar\rho')dl' + \int_\sigma g^\Omega\left(k^\Omega_{1L}, \bar\rho, \bar\rho'\right)\hat{n}'_1 \cdot \nabla'_t\psi^S_\beta(\bar\rho')dl'$$

$$- \sum_\alpha \frac{a^{(1)L}_{\beta\alpha}\psi^\Omega_\alpha(\bar\rho)}{(k^\Omega_\alpha)^2 - (k^\Omega_{1L})^2} + \sum_\alpha \frac{b^{(1)L}_{\beta\alpha}\psi^\Omega_\alpha(\bar\rho)}{(k^\Omega_\alpha)^2 - (k^\Omega_{1L})^2} + \sum_\alpha \frac{c^{(1)L}_{\beta\alpha}\psi^\Omega_\alpha(\bar\rho)}{(k^\Omega_\alpha)^2 - (k^\Omega_{1L})^2} = \begin{cases} \psi^S_{1\beta}(\bar\rho) & \bar\rho \in A_1 \\ 0 & \bar\rho \notin A_1 \end{cases} \tag{45}$$

$$- \int_{\partial S_3} \psi^S_\beta(\bar\rho')\,\hat{n}'_3 \cdot \nabla'_t g^\Omega\left(k^\Omega_{2L}, \bar\rho, \bar\rho'\right) dl' + \int_{\partial S_3} g^\Omega\left(k^\Omega_{2L}, \bar\rho, \bar\rho'\right)\hat{n}'_3 \cdot \nabla'_t\psi^S_\beta(\bar\rho')\, dl'$$

$$+ \sum_\alpha \frac{a^{(2)L}_{\beta\alpha}\psi^\Omega_\alpha(\bar\rho)}{(k^\Omega_\alpha)^2 - (k^\Omega_{2L})^2} - \sum_\alpha \frac{b^{(2)L}_{\beta\alpha}\psi^\Omega_\alpha(\bar\rho)}{(k^\Omega_\alpha)^2 - (k^\Omega_{2L})^2} = \begin{cases} \psi^S_{2\beta}(\bar\rho) & \bar\rho \in A_2 \\ 0 & \bar\rho \notin A_2 \end{cases} \tag{46}$$

By discretizing the surface integral equations in Eqs. (45)–(46) and using surface current notations $\bar{x}_\beta$, $\bar{y}_\beta$, $\bar{z}_\beta$, Eqs. (45) and (46) are rewritten as

$$\sum_n A^{(1)L}_{mn} x_{\beta n} - \sum_n B^{(1)L}_{mn} y_{\beta n} + \sum_n C^{(1)L}_{mn} z_{\beta n} - \sum_\alpha \frac{a^{(1)L}_{\beta\alpha}\psi^\Omega_\alpha(\bar\rho)}{(k^\Omega_\alpha)^2 - (k^\Omega_{1L})^2} + \sum_\alpha \frac{b^{(1)L}_{\beta\alpha}\psi^\Omega_\alpha(\bar\rho)}{(k^\Omega_\alpha)^2 - (k^\Omega_{1L})^2} + \sum_\alpha \frac{c^{(1)L}_{\beta\alpha}\psi^\Omega_\alpha(\bar\rho)}{(k^\Omega_\alpha)^2 - (k^\Omega_{1L})^2}$$

$$= \begin{cases} \psi^S_{1\beta}(\bar\rho) & \bar\rho \in A_1 \\ 0 & \bar\rho \notin A_1 \end{cases} \tag{47}$$

$$- \sum_n A^{(2)L}_{mn} x_{\beta n} + \sum_n B^{(2)L}_{mn} y_{\beta n} + \sum_\alpha \frac{a^{(2)L}_{\beta\alpha}\psi^\Omega_\alpha(\bar\rho)}{(k^\Omega_\alpha)^2 - (k^\Omega_{2L})^2} - \sum_\alpha \frac{b^{(2)L}_{\beta\alpha}\psi^\Omega_\alpha(\bar\rho)}{(k^\Omega_\alpha)^2 - (k^\Omega_{2L})^2} = \begin{cases} \psi^S_{2\beta}(\bar\rho) & \bar\rho \in A_2 \\ 0 & \bar\rho \notin A_2 \end{cases} \tag{48}$$

The surface currents, $\bar{x}_\beta$, $\bar{y}_\beta$, $\bar{z}_\beta$, are calculated via solving Eq. (31), while the modal coefficients $\bar{a}^{(1)L}_\beta$, $\bar{a}^{(2)L}_\beta$, $\bar{b}^{(1)L}_\beta$, $\bar{b}^{(2)L}_\beta$, $\bar{c}^{(1)L}_\beta$ are obtained from Eq. (42).

2.3. Orthonormalization of Modal Fields

Let β and β' be two different mode indices of waveguide S. The modal functions $\psi_{1\beta}^S$, $\psi_{1\beta'}^S$, $\psi_{2\beta}^S$, and $\psi_{2\beta'}^S$ satisfy the wave equation (2) with the respective modal wavenumbers $k_{1\beta}^S$, $k_{1\beta'}^S$, $k_{2\beta}^S$, and $k_{2\beta'}^S$. Applying Green's theorem and boundary condition (3), we obtain the orthogonality for $\beta \neq \beta'$.

$$\iint_{A_1} \psi_{1\beta}^S(\bar{\rho})\,\psi_{1\beta'}^S(\bar{\rho})\,d\bar{\rho} + \frac{\varepsilon_2}{\varepsilon_1}\iint_{A_2} \psi_{2\beta}^S(\bar{\rho})\,\psi_{2\beta'}^S(\bar{\rho})\,d\bar{\rho} = 0 \tag{49}$$

Setting $\beta' = \beta$ in (47) and (48) gives the mode normalization condition.

$$\iint_{A_1} \left|\psi_{1\beta}^S(\bar{\rho})\right|^2 d\bar{\rho} + \frac{\varepsilon_2}{\varepsilon_1}\iint_{A_2} \left|\psi_{2\beta}^S(\bar{\rho})\right|^2 d\bar{\rho} = 1 \tag{50}$$

Further taking Laplacian on Eqs. (47) and (48) and using the conditions:

$$\left(k_{1L}^\Omega\right)^2 \ll \left(k_{1\beta}^S\right)^2; \quad \left(k_{1L}^\Omega\right)^2 \ll \left(k_\alpha^\Omega\right)^2; \quad \left(k_{2L}^\Omega\right)^2 \ll \left(k_{2\beta}^S\right)^2; \quad \text{and } \left(k_{2L}^\Omega\right)^2 \ll \left(k_\alpha^\Omega\right)^2 \tag{51}$$

We derive the following normalization condition

$$\frac{1}{\left|k_{1\beta}^S\right|^4}\sum_\alpha \left(\left|-a_{\beta\alpha}^{(1)L} + b_{\beta\alpha}^{(1)L} + c_{\beta\alpha}^{(1)L}\right|^2 + \frac{\varepsilon_1}{\varepsilon_2}\left|-a_{\beta\alpha}^{(2)L} + b_{\beta\alpha}^{(2)L}\right|^2\right) = 1 \tag{52}$$

which can be easily and efficiently implemented. In numerical simulations, low wavenumbers k_{1L}^Ω and k_{2L}^Ω used are about 10^{-6} while mode wavenumbers $k_{1\beta}^S$, $k_{2\beta}^S$, and k_α^Ω are larger than 300. Thus the conditions in Eq. (51) are satisfied. After modal coefficients being normalized, Eq. (31) is used to find normalized surface currents. We can replace the modal coefficients and surface currents with the normalized ones in Eqs. (47) and (48). Then we have the normalized hybrid expressions for the modal functions.

2.4. Spurious Modes Rejection

Some of the eigenvalue solutions in the matrix equation (42) are spurious modes which are solutions of wave equation (2) but not physically existent. We apply an efficient spurious mode rejection method based on extinction theorem. Note that in Eq. (45), the left-hand side is zero when $\bar{\rho}$ is outside A_1. This suggests that we can set a threshold to check whether the extinction theorem is observed. Similar arguments apply to Eq. (46). The rejection of spurious modes is performed efficiently by using random coarse sampling in the respective regions. A physical mode gives finite nonzero values at the correct regions, and negligible values at other regions while spurious modes give non-small values in other regions as well as outside the waveguide S.

3. ACCELERATED CONVERGENCE OF BROADBAND GREEN'S FUNCTIONS

Given a source at $\bar{\rho}''$ in region 1, the Green's functions of waveguide S, $g_{11}^S(k_1, \bar{\rho}, \bar{\rho}'')$ and $g_{21}^S(k_2, \bar{\rho}, \bar{\rho}'')$ are expressed in modal representations as

$$g_{11}^S\left(k_1, \bar{\rho}, \bar{\rho}''\right) = \sum_\beta \frac{\psi_{1\beta}^S(\bar{\rho})\,\psi_{1\beta}^S(\bar{\rho}'')}{\left(k_{1\beta}^S\right)^2 - k_1^2} \tag{53}$$

$$g_{21}^S\left(k_2, \bar{\rho}, \bar{\rho}''\right) = \sum_\beta \frac{\psi_{2\beta}^S(\bar{\rho})\,\psi_{1\beta}^S(\bar{\rho}'')}{\left(k_{1\beta}^S\right)^2 - k_1^2} \tag{54}$$

The above expressions are exact but with a second order convergence as $1/(k_{1\beta}^S)^2$. The convergence is poor when the field points are close to the source point.

3.1. Green's Functions with 4th Order Convergence

With the extractions of low wavenumber Green's functions $g_{11}^S(k_{1L}^S, \bar{\rho}, \bar{\rho}'')$ and $g_{21}^S(k_{2L}^S, \bar{\rho}, \bar{\rho}'')$, $g_{11}^S(k_1, \bar{\rho}, \bar{\rho}'')$ and $g_{21}^S(k_2, \bar{\rho}, \bar{\rho}'')$ are expressed as, respectively.

$$g_{11}^S\left(k_1, \bar{\rho}, \bar{\rho}''\right) = g_{11}^S\left(k_{1L}^S, \bar{\rho}, \bar{\rho}''\right) + \sum_\beta \frac{\left[k_1^2 - \left(k_{1L}^S\right)^2\right]\psi_{1\beta}^S\left(\bar{\rho}''\right)}{\left[\left(k_{1\beta}^S\right)^2 - k_1^2\right]\left[\left(k_{1\beta}^S\right)^2 - \left(k_{1L}^S\right)^2\right]}\psi_{1\beta}^S\left(\bar{\rho}\right) \tag{55}$$

$$g_{21}^S\left(k_2, \bar{\rho}, \bar{\rho}''\right) = g_{21}^S\left(k_{2L}^S, \bar{\rho}, \bar{\rho}''\right) + \sum_\beta \frac{\left[k_1^2 - \left(k_{1L}^S\right)^2\right]\psi_{1\beta}^S\left(\bar{\rho}''\right)}{\left[\left(k_{1\beta}^S\right)^2 - k_1^2\right]\left[\left(k_{1\beta}^S\right)^2 - \left(k_{1L}^S\right)^2\right]}\psi_{2\beta}^S\left(\bar{\rho}\right) \tag{56}$$

The modal summations in Eqs. (55) and (56) have an improved convergence rate of $1/(k_{1\beta}^S)^4$. The low wavenumber Green's functions $g_{11}^S(k_{1L}^S, \bar{\rho}, \bar{\rho}'')$ and $g_{21}^S(k_{2L}^S, \bar{\rho}, \bar{\rho}'')$, are calculated by using direct MoM.

Using the Green's theorem and boundary conditions in region 1, we derive the integral equation for $g_{11}^S(k_1, \bar{\rho}, \bar{\rho}'')$.

$$g_0\left(k_1, \bar{\rho}, \bar{\rho}''\right) + \int_{\partial S_1} J_3\left(k_1, \bar{\rho}'\right) g_0\left(k_1, \bar{\rho}, \bar{\rho}'\right) dl' + \int_{\partial S_3} J_1\left(k_1, \bar{\rho}'\right) \hat{n}_3' \cdot \nabla_t' g_0\left(k_1, \bar{\rho}, \bar{\rho}'\right) dl'$$
$$- \int_{\partial S_3} J_2\left(k_1, \bar{\rho}'\right) g_0\left(k_1, \bar{\rho}, \bar{\rho}'\right) dl' = \begin{cases} g_{11}^S\left(k_1, \bar{\rho}, \bar{\rho}''\right) & \bar{\rho} \in A_1 \\ 0 & \bar{\rho} \notin A_1 \end{cases} \tag{57}$$

where the surface currents $J_1(k_1, \bar{\rho}')$ and $J_2(k_1, \bar{\rho}')$ are on ∂S_3,

$$J_1\left(k_1, \bar{\rho}'\right) = g_{11}^S\left(k_1, \bar{\rho}', \bar{\rho}''\right) \tag{58}$$
$$J_2\left(k_1, \bar{\rho}'\right) = \hat{n}_3' \cdot \nabla_t' g_{11}^S\left(k_1, \bar{\rho}', \bar{\rho}''\right) \tag{59}$$

and $J_3(k_1, \bar{\rho}')$ is on ∂S_1.

$$J_3\left(k_1, \bar{\rho}'\right) = \hat{n}_1' \cdot \nabla_t' g_{11}^S\left(k_1, \bar{\rho}', \bar{\rho}''\right) \tag{60}$$

In region 2, we derive similar integral equation for $g_{21}^S(k_2, \bar{\rho}, \bar{\rho}'')$.

$$- \int_{\partial S_3} J_1\left(k_1, \bar{\rho}'\right) \hat{n}_3' \cdot \nabla_t' g_0\left(k_2, \bar{\rho}, \bar{\rho}'\right) dl' + \int_{\partial S_3} J_2\left(k_1, \bar{\rho}'\right) g_0\left(k_2, \bar{\rho}, \bar{\rho}'\right) dl'$$
$$+ \int_{\partial S_2} J_4\left(k_2, \bar{\rho}'\right) g_0\left(k_2, \bar{\rho}, \bar{\rho}'\right) dl' = \begin{cases} g_{21}^S\left(k_2, \bar{\rho}, \bar{\rho}''\right) & \bar{\rho} \in A_2 \\ 0 & \bar{\rho} \notin A_2 \end{cases} \tag{61}$$

where the surface current $J_4(k_1, \bar{\rho}')$ is on ∂S_2.

$$J_4\left(k_2, \bar{\rho}'\right) = \hat{n}_2' \cdot \nabla_t' g_{21}^S\left(k_2, \bar{\rho}', \bar{\rho}''\right) \tag{62}$$

Setting $k_1 = k_{1L}^S$ and $\bar{\rho}'$ outside A_1 in Eq. (57), we have

$$-g_0\left(k_{1L}^S, \bar{\rho}, \bar{\rho}''\right) = \int_{\partial S_1} J_3\left(k_{1L}^S, \bar{\rho}'\right) g_0\left(k_{1L}^S, \bar{\rho}, \bar{\rho}'\right) dl' + \int_{\partial S_3} J_1\left(k_{1L}^S, \bar{\rho}'\right) \hat{n}_3' \cdot \nabla_t' g_0\left(k_{1L}^S, \bar{\rho}, \bar{\rho}'\right) dl'$$
$$- \int_{\partial S_3} J_2\left(k_{1L}^S, \bar{\rho}'\right) g_0\left(k_{1L}^S, \bar{\rho}, \bar{\rho}'\right) dl' \tag{63}$$

Similarly, let $k_2 = k_{2L}^S$, $k_1 = k_{1L}^S$, $\bar{\rho}'$ be outside A_2 in Eq. (61), we get

$$0 = - \int_{\partial S_3} J_1\left(k_{1L}^S, \bar{\rho}'\right) \hat{n}_3' \cdot \nabla_t' g_0\left(k_{2L}^S, \bar{\rho}, \bar{\rho}'\right) dl' + \int_{\partial S_3} J_2\left(k_{1L}^S, \bar{\rho}'\right) g_0\left(k_{2L}^S, \bar{\rho}, \bar{\rho}'\right) dl'$$
$$+ \int_{\partial S_2} J_4\left(k_{1L}^S, \bar{\rho}'\right) g_0\left(k_{2L}^S, \bar{\rho}, \bar{\rho}'\right) dl' \tag{64}$$

The coupled integral equations, Eqs. (63) and (64), are discretized using pulse basis function and point matching method. We obtain the following matrix equation.

$$\overline{\overline{Z}}_L \bar{J}_L = \bar{g}_L \tag{65}$$

In (65), the column vector $\bar{J}_L$ contains surface currents,

$$\bar{J}_L = \begin{bmatrix} \bar{J}_1 & \bar{J}_2 & \bar{J}_3 & \bar{J}_4 \end{bmatrix}^T \tag{66}$$

and $\overline{\overline{Z}}_L$ is the impedance matrix with matrix elements,

$$\overline{\overline{Z}}_L = \begin{bmatrix} -\overline{\overline{A}}_{M3}^{(1)L} & \overline{\overline{B}}_{M3}^{(1)L} & -\overline{\overline{C}}_{M3}^{(1)L} & \overline{\overline{0}} \\ \overline{\overline{A}}_{M3}^{(2)L} & -\overline{\overline{B}}_{M3}^{(2)L} & \overline{\overline{0}} & -\overline{\overline{C}}_{M3}^{(2)L} \\ -\overline{\overline{A}}_{M1}^{(1)L} & \overline{\overline{B}}_{M1}^{(1)L} & -\overline{\overline{C}}_{M1}^{(1)L} & \overline{\overline{0}} \\ \overline{\overline{A}}_{M2}^{(2)L} & -\overline{\overline{B}}_{M2}^{(2)L} & \overline{\overline{0}} & -\overline{\overline{C}}_{M2}^{(2)L} \end{bmatrix} \tag{67}$$

with the expressions of matrix elements given by

$$A_{M3,mn}^{(1)L} = \int_{\partial S_3^{(n)}} \hat{n}_3' \cdot \nabla_t' g_0 \left(k_{1L}^S, \bar{\rho}_m^{\partial S_3}, \bar{\rho}' \right) dl' \tag{68}$$

$$B_{M3,mn}^{(1)L} = \int_{\partial S_3^{(n)}} g_0 \left(k_{1L}^S, \bar{\rho}_m^{\partial S_3}, \bar{\rho}' \right) dl' \tag{69}$$

$$C_{M3,mn}^{(1)L} = \int_{\partial S_1^{(n)}} g_0 \left(k_{1L}^S, \bar{\rho}_m^{\partial S_3}, \bar{\rho}' \right) dl' \tag{70}$$

$$A_{M3,mn}^{(2)L} = \int_{\partial S_3^{(n)}} \hat{n}_3' \cdot \nabla_t' g_0 \left(k_{2L}^S, \bar{\rho}_m^{\partial S_3}, \bar{\rho}' \right) dl' \tag{71}$$

$$B_{M3,mn}^{(2)L} = \int_{\partial S_3^{(n)}} g_0 \left(k_{2L}^S, \bar{\rho}_m^{\partial S_3}, \bar{\rho}' \right) dl' \tag{72}$$

$$C_{M3,mn}^{(2)L} = \int_{\partial S_1^{(n)}} g_0 \left(k_{2L}^S, \bar{\rho}_m^{\partial S_3}, \bar{\rho}' \right) dl' \tag{73}$$

$$A_{M1,mn}^{(1)L} = \int_{\partial S_3^{(n)}} \hat{n}_3' \cdot \nabla_t' g_0 \left(k_{1L}^S, \bar{\rho}_m^{\partial S_1}, \bar{\rho}' \right) dl' \tag{74}$$

$$B_{M1,mn}^{(1)L} = \int_{\partial S_3^{(n)}} g_0 \left(k_{1L}^S, \bar{\rho}_m^{\partial S_1}, \bar{\rho}' \right) dl' \tag{75}$$

$$C_{M1,mn}^{(1)L} = \int_{\partial S_1^{(n)}} g_0 \left(k_{1L}^S, \bar{\rho}_m^{\partial S_1}, \bar{\rho}' \right) dl' \tag{76}$$

$$A_{M2,mn}^{(2)L} = \int_{\partial S_3^{(n)}} \hat{n}_3' \cdot \nabla_t' g_0 \left(k_{2L}^S, \bar{\rho}_m^{\partial S_2}, \bar{\rho}' \right) dl' \tag{77}$$

$$B_{M2,mn}^{(2)L} = \int_{\partial S_3^{(n)}} g_0 \left(k_{2L}^S, \bar{\rho}_m^{\partial S_2}, \bar{\rho}' \right) dl' \tag{78}$$

$$C_{M2,mn}^{(2)L} = \int_{\partial S_1^{(n)}} g_0 \left(k_{2L}^S, \bar{\rho}_m^{\partial S_2}, \bar{\rho}' \right) dl' \tag{79}$$

The column vector $\bar{g}_L$ in (65) is given as

$$\bar{g}_L = \begin{bmatrix} \bar{g}_3^{(1)} & \bar{0} & \bar{g}_1^{(1)} & \bar{0} \end{bmatrix}^T \tag{80}$$

where

$$g_{3m}^{(1)} = g_0 \left(k_1, \bar{\rho}_m^{\partial S_3}, \bar{\rho}'' \right) \tag{81}$$

$$g_{1m}^{(1)} = g_0 \left(k_1, \bar{\rho}_m^{\partial S_1}, \bar{\rho}'' \right) \tag{82}$$

After solving $J_1(k_{1L}^S, \bar{\rho}')$, $J_2(k_{1L}^S, \bar{\rho}')$, $J_3(k_{1L}^S, \bar{\rho}')$, and $J_4(k_{2L}^S, \bar{\rho}')$ from Eq. (65), we use Eqs. (83) and (84) to calculate the Green's functions at low wavenumbers $g_{11}^S(k_{1L}^S, \bar{\rho}, \bar{\rho}'')$ and $g_{21}^S(k_{2L}^S, \bar{\rho}, \bar{\rho}'')$, respectively.

$$g_{11}^S\left(k_{1L}^S, \bar{\rho}, \bar{\rho}''\right) = g_0\left(k_{1L}^S, \bar{\rho}, \bar{\rho}'\right) + \int_{\partial S_1} J_3\left(k_{1L}^S, \bar{\rho}'\right) g_0\left(k_{1L}^S, \bar{\rho}, \bar{\rho}'\right) dl'$$

$$+ \int_{\partial S_3} J_1\left(k_{1L}^S, \bar{\rho}'\right) \hat{n}_3' \cdot \nabla_t' g_0\left(k_{1L}^S, \bar{\rho}, \bar{\rho}'\right) dl' - \int_{\partial S_3} J_2\left(k_{1L}^S, \bar{\rho}'\right) g_0\left(k_{1L}^S, \bar{\rho}, \bar{\rho}'\right) dl' \quad (83)$$

$$g_{21}^S\left(k_{2L}^S, \bar{\rho}, \bar{\rho}''\right) = \int_{\partial S_2} J_4\left(k_{1L}^S, \bar{\rho}'\right) g_0\left(k_{2L}^S, \bar{\rho}, \bar{\rho}'\right) dl' - \int_{\partial S_3} J_1\left(k_{1L}^S, \bar{\rho}'\right) \hat{n}_3' \cdot \nabla_t' g_0\left(k_{2L}^S, \bar{\rho}, \bar{\rho}'\right) dl'$$

$$+ \int_{\partial S_3} J_2\left(k_{1L}^S, \bar{\rho}'\right) g_0\left(k_{2L}^S, \bar{\rho}, \bar{\rho}'\right) dl' \quad (84)$$

Note that k_{1L}^S and k_{2L}^S are chosen such that $k_{1L}^\Omega \ll k_{1L}^S \ll k$ and $k_{2L}^\Omega \ll k_{2L}^S \ll k$. Eqs. (83) and (84) for $g_{11}^S(k_{1L}^S, \bar{\rho}, \bar{\rho}'')$ and $g_{21}^S(k_{2L}^S, \bar{\rho}, \bar{\rho}'')$ are calculated only one time.

3.2. Wavenumber Derivatives for Green's Functions with 6th Order Convergence

An algorithm with higher order convergence rate can reduce the required number of higher order modes in mode summations. We have developed two methods for homogeneous irregular shape waveguide Green's functions with sixth order convergence [14, 15]. One is based on finite difference method [14] and the other is based on the derivative of current with respect to wavenumber [15]. In this section, we use the wavenumber derivative method to the inhomogeneous waveguide case.

We write Green's functions $g_{11}^S(k_1^S, \bar{\rho}, \bar{\rho}'')$ and $g_{21}^S(k_2^S, \bar{\rho}, \bar{\rho}'')$ as follows.

$$g_{11}^S\left(k_1, \bar{\rho}, \bar{\rho}''\right) = g_{11}^S\left(k_{1L}^S, \bar{\rho}, \bar{\rho}''\right) + \left[k_1^2 - \left(k_{1L}^S\right)^2\right] \left[\frac{\partial g_{11}^S\left(k_1, \bar{\rho}, \bar{\rho}''\right)}{\partial k_1^2}\right]_{k_1 = k_{1L}^S}$$

$$+ \sum_\beta \frac{\left[k_1^2 - \left(k_{1L}^S\right)^2\right]^2 \psi_{1\beta}^S\left(\bar{\rho}''\right) \psi_{1\beta}^S\left(\bar{\rho}\right)}{\left[\left(k_{1\beta}^S\right)^2 - k_1^2\right] \left[\left(k_{1\beta}^S\right)^2 - \left(k_{1L}^S\right)^2\right]^2} \quad (85)$$

$$g_{21}^S\left(k_2, \bar{\rho}, \bar{\rho}''\right) = g_{21}^S\left(k_{2L}^S, \bar{\rho}, \bar{\rho}''\right) + \left[k_2^2 - \left(k_{2L}^S\right)^2\right] \left[\frac{\partial g_{21}^S\left(k_2, \bar{\rho}, \bar{\rho}''\right)}{\partial k_2^2}\right]_{k_2 = k_{2L}^S}$$

$$+ \sum_\beta \frac{\left[k_2^2 - \left(k_{2L}^S\right)^2\right]^2 \psi_{1\beta}^S\left(\bar{\rho}''\right) \psi_{1\beta}^S\left(\bar{\rho}\right)}{\left[\left(k_{1\beta}^S\right)^2 - k_2^2\right] \left[\left(k_{1\beta}^S\right)^2 - \left(k_{2L}^S\right)^2\right]^2} \quad (86)$$

where the Green's functions are expressed in terms of the derivatives of Green's functions at low wavenumbers that are calculated using MoM.

The derivatives of Green's functions are obtained from Eqs. (57) and (61). Let $\bar{\rho}$ be inside A_1 in Eq. (57). Taking derivative with respective to wavenumbers and setting $k_1 = k_{1L}^S$ yield

$$\left[\frac{\partial g_{11}^S\left(k_1, \bar{\rho}, \bar{\rho}''\right)}{\partial k_1^2}\right]_{k_1 = k_{1L}^S}$$

$$= \left[\frac{\partial g_0(k_1, \bar{\rho}, \bar{\rho}'')}{\partial k_1^2}\right]_{k_1 = k_{1L}^S} + \int_{\partial S_1} J_{3L}^d\left(k_{1L}^S, \bar{\rho}'\right) g_0\left(k_{1L}^S, \bar{\rho}, \bar{\rho}'\right) dl' + \int_{\partial S_1} J_3\left(k_{1L}^S, \bar{\rho}'\right) \left[\frac{\partial g_0(k_1, \bar{\rho}, \bar{\rho}')}{\partial k_1^2}\right]_{k_1 = k_{1L}^S} dl'$$

$$+ \int_{\partial S_3} J_{1L}^d\left(k_{1L}^S, \bar{\rho}'\right) \hat{n}_3' \cdot \nabla_t' g_0\left(k_{1L}^S, \bar{\rho}, \bar{\rho}'\right) dl' + \int_{\partial S_3} J_1\left(k_{1L}^S, \bar{\rho}'\right) \left[\frac{\partial \hat{n}_3' \cdot \nabla_t' g_0\left(k_1, \bar{\rho}, \bar{\rho}'\right)}{\partial k_1^2}\right]_{k_1 = k_{1L}^S} dl'$$

$$- \int_{\partial S_3} J_{2L}^d\left(k_{1L}^S, \bar{\rho}'\right) g_0\left(k_{1L}^S, \bar{\rho}, \bar{\rho}'\right) dl' - \int_{\partial S_3} J_2\left(k_{1L}^S, \bar{\rho}'\right) \left[\frac{\partial g_0\left(k_1, \bar{\rho}, \bar{\rho}'\right)}{\partial k_1^2}\right]_{k_1 = k_{1L}^S} dl' \quad (87)$$

where

$$J_{1L}^d \left(k_{1L}^S, \bar{\rho}' \right) = \left[\frac{\partial J_1 \left(k_1, \bar{\rho}' \right)}{\partial k_1^2} \right]_{k_1 = k_{1L}^S} \tag{88}$$

$$J_{2L}^d \left(k_{1L}^S, \bar{\rho}' \right) = \left[\frac{\partial J_2 \left(k_1, \bar{\rho}' \right)}{\partial k_1^2} \right]_{k_1 = k_{1L}^S} \tag{89}$$

$$J_{3L}^d \left(k_{1L}^S, \bar{\rho}' \right) = \left[\frac{\partial J_3 \left(k_1, \bar{\rho}' \right)}{\partial k_1^2} \right]_{k_1 = k_{1L}^S} \tag{90}$$

Similarly, let $\bar{\rho}$ be inside A_2 in Eq. (61). Taking derivative with respective to wavenumbers and setting $k_2 = k_{2L}^S$ and $k_1 = k_{1L}^S$ yield

$$\left[\frac{\partial g_{21}^S \left(k_2, \bar{\rho}, \bar{\rho}'' \right)}{\partial k_2^2} \right]_{k_2 = k_{2L}^S} = \int_{\partial S_2} J_{4L}^d \left(k_{2L}^S, \bar{\rho}' \right) g_0 \left(k_{2L}^S, \bar{\rho}, \bar{\rho}' \right) dl' + \int_{\partial S_2} J_4 \left(k_{1L}^S, \bar{\rho}' \right) \left[\frac{\partial g_0 \left(k_2, \bar{\rho}, \bar{\rho}' \right)}{\partial k_2^2} \right]_{k_2 = k_{2L}^S} dl'$$

$$- \int_{\partial S_3} J_{1L}^d \left(k_{1L}^S, \bar{\rho}' \right) \hat{n}_3' \cdot \nabla_t' g_0 \left(k_{2L}^S, \bar{\rho}, \bar{\rho}' \right) dl'$$

$$- \int_{\partial S_3} J_1 \left(k_{1L}^S, \bar{\rho}' \right) \left[\frac{\partial \hat{n}_3' \cdot \nabla_t' g_0 \left(k_2, \bar{\rho}, \bar{\rho}' \right)}{\partial k_2^2} \right]_{k_2 = k_{2L}^S} dl'$$

$$+ \int_{\partial S_3} J_{2L}^d \left(k_{1L}^S, \bar{\rho}' \right) g_0 \left(k_{2L}^S, \bar{\rho}, \bar{\rho}' \right) dl' + \int_{\partial S_3} J_2 \left(k_{1L}^S, \bar{\rho}' \right) \left[\frac{\partial g_0 \left(k_2, \bar{\rho}, \bar{\rho}' \right)}{\partial k_2^2} \right]_{k_2 = k_{2L}^S} dl' \tag{91}$$

where

$$J_{4L}^d \left(k_{2L}^S, \bar{\rho}' \right) = \left[\frac{\partial J_4 \left(k_2, \bar{\rho}' \right)}{\partial k_2^2} \right]_{k_2 = k_{2L}^S} \tag{92}$$

To compute the derivatives of currents, we use the extended boundary conditions in Eqs. (57) and (61). In Eq. (57), let $\bar{\rho}$ be outside A_1 and take wavenumber derivatives, we have

$$- \int_{\partial S_3} J_{1L}^d \left(k_{1L}^S, \bar{\rho}' \right) \hat{n}_3' \cdot \nabla_t' g_0 \left(k_{1L}^S, \bar{\rho}, \bar{\rho}' \right) dl' + \int_{\partial S_3} J_{2L}^d \left(k_{1L}^S, \bar{\rho}' \right) g_0 \left(k_{1L}^S, \bar{\rho}, \bar{\rho}' \right) dl'$$

$$- \int_{\partial S_1} J_{3L}^d \left(k_{1L}^S, \bar{\rho}' \right) g_0 \left(k_{1L}^S, \bar{\rho}, \bar{\rho}' \right) dl'$$

$$= \left[\frac{\partial g_0 \left(k_1, \bar{\rho}, \bar{\rho}'' \right)}{\partial k_1^2} \right]_{k_1 = k_{1L}^S} + \int_{\partial S_1} J_3 \left(k_{1L}^S, \bar{\rho}' \right) \left[\frac{\partial g_0 \left(k_1, \bar{\rho}, \bar{\rho}' \right)}{\partial k_1^2} \right]_{k_1 = k_{1L}^S} dl'$$

$$+ \int_{\partial S_3} J_1 \left(k_{1L}^S, \bar{\rho}' \right) \left[\frac{\partial \hat{n}_3' \cdot \nabla_t' g_0 \left(k_1, \bar{\rho}, \bar{\rho}' \right)}{\partial k_1^2} \right]_{k_1 = k_{1L}^S} dl'$$

$$- \int_{\partial S_3} J_2 \left(k_{1L}^S, \bar{\rho}' \right) \left[\frac{\partial g_0 \left(k_1, \bar{\rho}, \bar{\rho}' \right)}{\partial k_1^2} \right]_{k_1 = k_{1L}^S} dl' \tag{93}$$

Similarly, let $\bar{\rho}$ be outside A_2 in Eq. (61) and take wavenumber derivatives, we obtain

$$\int_{\partial S_3} J_{1L}^d \left(k_{1L}^S, \bar{\rho}' \right) \hat{n}_3' \cdot \nabla_t' g_0 \left(k_{2L}^S, \bar{\rho}, \bar{\rho}' \right) dl' - \int_{\partial S_3} \left[\frac{\partial J_2 \left(k_1, \bar{\rho}' \right)}{\partial k_1^2} \right]_{k_1 = k_{1L}^S} g_0 \left(k_{2L}^S, , \bar{\rho}, \bar{\rho}' \right) dl'$$

$$- \int_{\partial S_2} \left[\frac{\partial J_4 \left(k_1, \bar{\rho}' \right)}{\partial k_1^2} \right]_{k_1 = k_{1L}^S} g_0 \left(k_{2L}^S, , \bar{\rho}, \bar{\rho}' \right) dl'$$

$$= - \int_{\partial S_3} J_1 \left(k_{1L}^S, , \bar{\rho}' \right) \left[\frac{\partial \hat{n}_3' \cdot \nabla_t' g_0 \left(k_2, \bar{\rho}, \bar{\rho}' \right)}{\partial k_2^2} \right]_{k_2 = k_{2L}^S} dl' - \int_{\partial S_3} J_2 \left(k_{2L}^S, , \bar{\rho}' \right) \left[\frac{\partial g_0 \left(k_2, \bar{\rho}, \bar{\rho}' \right)}{\partial k_2^2} \right]_{k_2 = k_{2L}^S} dl'$$

$$\int_{\partial S_2} J_4 \left(k_{1L}^S, , \bar{\rho}' \right) \left[\frac{\partial g_0 \left(k_2, \bar{\rho}, \bar{\rho}' \right)}{\partial k_2^2} \right]_{k_2 = k_{2L}^S} dl' \tag{94}$$

Pulse basis function and point matching method are used to discretize the coupled integral equations (93) and (94). We obtain the following matrix equation (95).

$$\overline{\overline{Z}}_L \bar{J}_L^d = \bar{g}_L^d + \overline{\overline{Z}}_L^d \bar{J}_L \tag{95}$$

In Eq. (95), $\bar{J}_L^d$ is the column vector containing all current derivatives,

$$\bar{J}_L^d = \begin{bmatrix} \bar{J}_{1L}^d & \bar{J}_{2L}^d & \bar{J}_{3L}^d & \bar{J}_{4L}^d \end{bmatrix}^T \tag{96}$$

and $\overline{\overline{Z}}_L^d$ is the matrix with matrix elements,

$$\overline{\overline{Z}}_L^d = \begin{bmatrix} \overline{\overline{A}}_{M3}^{d(1)L} & -\overline{\overline{B}}_{M3}^{d(1)L} & \overline{\overline{C}}_{M3}^{d(1)L} & \overline{\overline{0}} \\ -\overline{\overline{A}}_{M3}^{d(2)L} & \overline{\overline{B}}_{M3}^{d(2)L} & \overline{\overline{0}} & \overline{\overline{C}}_{M3}^{d(2)L} \\ \overline{\overline{A}}_{M1}^{d(1)L} & -\overline{\overline{B}}_{M1}^{d(1)L} & \overline{\overline{C}}_{M1}^{d(1)L} & \overline{\overline{0}} \\ -\overline{\overline{A}}_{M2}^{d(2)L} & \overline{\overline{B}}_{M2}^{d(2)L} & \overline{\overline{0}} & \overline{\overline{C}}_{M2}^{d(2)L} \end{bmatrix} \tag{97}$$

with the expressions of matrix elements given by

$$A_{M3,mn}^{d(1)L} = \int_{\partial S_3^{(n)}} \left[\frac{\partial \hat{n}_3' \cdot \nabla_t' g_0 \left(k_1, \bar{\rho}_m^{\partial S_3}, \bar{\rho}' \right)}{\partial k_1^2} \right]_{k_1 = k_{1L}^S} dl' \tag{98}$$

$$B_{M3,mn}^{d(1)L} = \int_{\partial S_3^{(n)}} \left[\frac{\partial g_0 \left(k_1, \bar{\rho}_m^{\partial S_3}, \bar{\rho}' \right)}{\partial k_1^2} \right]_{k_1 = k_{1L}^S} dl' \tag{99}$$

$$C_{M3,mn}^{d(1)L} = \int_{\partial S_1^{(n)}} \left[\frac{\partial g_0 \left(k_1, \bar{\rho}_m^{\partial S_3}, \bar{\rho}' \right)}{\partial k_1^2} \right]_{k_1 = k_{1L}^S} dl' \tag{100}$$

$$A_{M3,mn}^{d(2)L} = \int_{\partial S_3^{(n)}} \left[\frac{\partial \hat{n}_3' \cdot \nabla_t' g_0 \left(k_2, \bar{\rho}_m^{\partial S_3}, \bar{\rho}' \right)}{\partial k_1^2} \right]_{k_1 = k_{1L}^S} dl' \tag{101}$$

$$B_{M3,mn}^{d(2)L} = \int_{\partial S_3^{(n)}} \left[\frac{\partial g_0 \left(k_2, \bar{\rho}_m^{\partial S_3}, \bar{\rho}' \right)}{\partial k_1^2} \right]_{k_1 = k_{1L}^S} dl' \tag{102}$$

$$C_{M3,mn}^{d(2)L} = \int_{\partial S_1^{(n)}} \left[\frac{\partial g_0 \left(k_2, \bar{\rho}_m^{\partial S_3}, \bar{\rho}' \right)}{\partial k_1^2} \right]_{k_1 = k_{1L}^S} dl' \tag{103}$$

$$A_{M1,mn}^{d(1)L} = \int_{\partial S_3^{(n)}} \left[\frac{\partial \hat{n}_3' \cdot \nabla_t' g_0 \left(k_1, \bar{\rho}_m^{\partial S_1}, \bar{\rho}' \right)}{\partial k_1^2} \right]_{k_1 = k_{1L}^S} dl' \tag{104}$$

$$B_{M1,mn}^{d(1)L} = \int_{\partial S_3^{(n)}} \left[\frac{\partial g_0 \left(k_1, \bar{\rho}_m^{\partial S_1}, \bar{\rho}' \right)}{\partial k_1^2} \right]_{k_1 = k_{1L}^S} dl' \tag{105}$$

$$C_{M1,mn}^{d(1)L} = \int_{\partial S_1^{(n)}} \left[\frac{\partial g_0 \left(k_1, \bar{\rho}_m^{\partial S_1}, \bar{\rho}' \right)}{\partial k_1^2} \right]_{k_1 = k_{1L}^S} dl' \tag{106}$$

$$A_{M2,mn}^{d(2)L} = \int_{\partial S_3^{(n)}} \left[\frac{\partial \hat{n}_3' \cdot \nabla_t' g_0 \left(k_2, \bar{\rho}_m^{\partial S_2}, \bar{\rho}' \right)}{\partial k_1^2} \right]_{k_1 = k_{1L}^S} dl' \tag{107}$$

$$B_{M2,mn}^{d(2)L} = \int_{\partial S_3^{(n)}} \left[\frac{\partial g_0 \left(k_2, \bar{\rho}_m^{\partial S_2}, \bar{\rho}' \right)}{\partial k_1^2} \right]_{k_1 = k_{1L}^S} dl' \tag{108}$$

$$C_{M2,mn}^{d(2)L} = \int_{\partial S_1^{(n)}} \left[\frac{\partial g_0\left(k_2, \bar{\rho}_m^{\partial S_2}, \bar{\rho}'\right)}{\partial k_1^2} \right]_{k_1 = k_{1L}^S} dl' \tag{109}$$

The column vector $\bar{g}_L^d$ in (95) is defined as

$$\bar{g}_L^d = \left[\begin{array}{cccc} \bar{g}_3^{d(1)L} & \bar{0} & \bar{g}_1^{d(1)L} & \bar{0} \end{array} \right]^T \tag{110}$$

where

$$g_{3m}^{d(1)L} = \left[\frac{\partial g_0\left(k_1, \bar{\rho}_m^{\partial S_3}, \bar{\rho}''\right)}{\partial k_1^2} \right]_{k_1 = k_{1L}^S} \tag{111}$$

$$g_{1m}^{d(1)L} = \left[\frac{\partial g_0\left(k_1, \bar{\rho}_m^{\partial S_1}, \bar{\rho}''\right)}{\partial k_1^2} \right]_{k_1 = k_{1L}^S} \tag{112}$$

We note that $\bar{J}_L$ and $\bar{\bar{Z}}_L$ in Eq. (95) are the same as those given in Eqs. (66) and (67), respectively. Thus both currents $\bar{J}_L$ and current derivatives $\bar{J}_L^d$ have the same low wavenumber impedance matrices. After solving $\bar{J}_L$ and $\bar{J}_L^d$, we use Eqs. (87) and (91) to evaluate wavenumber derivative of Green's functions at any location $\bar{\rho}$.

4. NUMERICAL RESULTS

The dimensions of waveguide S in Figure 1 are $L_x = L_y = 500$ mils. The rectangular cut σ has widths $W_x = 100$ mils and $W_y = 250$ mils. The waveguide S is filled with two lossless dielectrics $\varepsilon_1 = 4.41\varepsilon_0$ and $\varepsilon_2 = 2.25\varepsilon_0$. The horizontal interface ∂S_3 is at $y = -50$ mils. Perfect electric conductor (PEC) boundaries of TM modes, corresponding to Dirichelt boundary conditions are imposed on ∂S_1 and ∂S_2.

4.1. Resonant Frequencies and Modal Functions

We first illustrate the modal solutions of the irregularly shaped waveguide S including resonant frequencies and normalized mode fields. We use $390\psi_\alpha^\Omega$'s, $\alpha = 1, 2, \ldots, 390$, to form the matrix elements of $\bar{\bar{P}}^L$ in (41), and set the low wavenumber k_{1L}^Ω equal to $10^{-6}(f_L^\Omega = 22.72\,\text{Hz})$. From the eigen-values of $\bar{\bar{P}}^L$, we calculate the resonant wavenumbers $k_{1\beta}^S$ and resonant frequencies. Table 1 shows the first 10 resonant frequencies for the modes of waveguide S. We also compare the results of direct MoM and HFSS. The results of BBGFL are in good agreement with the other two methods.

Table 1. First 10 resonant frequencies of waveguide S.

β	$BBGFL$	MoM	$HFSS$
1	9.40 GHz	9.40 GHz	9.40 GHz
2	14.76 GHz	14.76 GHz	14.76 GHz
3	15.64 GHz	15.65 GHz	15.64 GHz
4	19.21 GHz	19.21 GHz	19.21 GHz
5	20.67 GHz	20.68 GHz	20.67 GHz
6	22.15 GHz	22.15 GHz	22.15 GHz
7	23.56 GHz	23.56 GHz	23.55 GHz
8	25.80 GHz	25.80 GHz	25.80 GHz
9	26.16 GHz	26.16 GHz	26.16 GHz
10	27.82 GHz	27.82 GHz	27.82 GHz

The eigen-vector $\bar{v}_\beta^L$ in Eq. (42) has the expansion coefficients of modal functions which are used to construct modal field functions. The modal function ψ_β^S of waveguide S consists of $\psi_{1\beta}^S$ of region 1 and $\psi_{2\beta}^S$ of regions 2. Figure 2 shows the first five normalized modal functions. The results of $\psi_{1\beta}^S$, in the top row, and $\psi_{2\beta}^S$, in the middle row, are in agreement with the extinction theorem. The modal functions ψ_β^S are smooth across the dielectric interface ∂S_3 when $\psi_{1\beta}^S$ and $\psi_{2\beta}^S$ are combined in the bottom row of Figure 2.
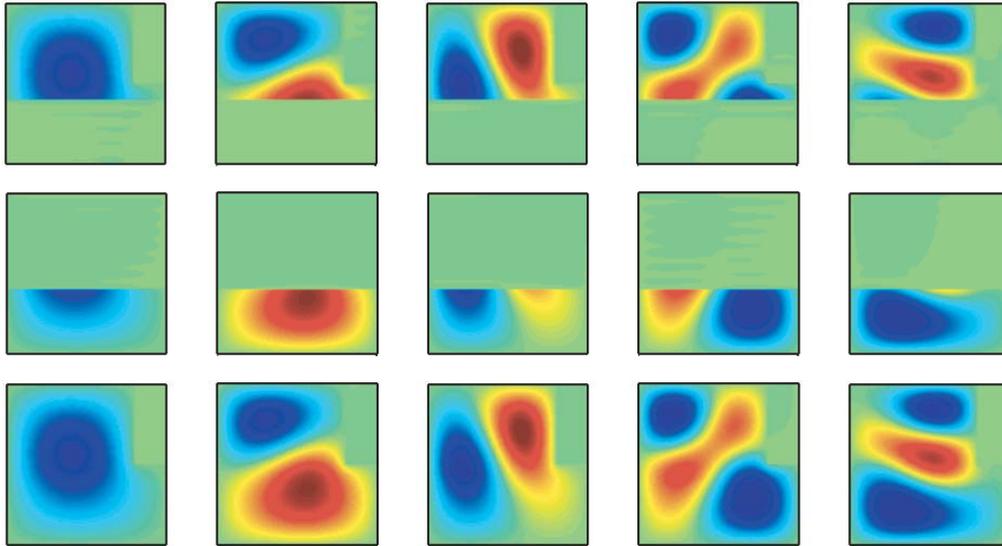
Figure 2. First 5 modal functions, from left to right. Top row: $\psi_{1\beta}^S$; Middle row: $\psi_{2\beta}^S$; and Bottom row: ψ_β^S.

In Figure 3, we plot the first 10 modal surface currents $\bar{z}_\beta$ on σ using BBGFL and compare with those computed using the direct MoM. The BBGFL results are in good agreement with those of direct MoM, even at locations near the corner as denoted by the dot line. We compare the modal surface currents $\bar{x}_\beta$ and $\bar{y}_\beta$ on the interface ∂S_3 with those of MoM in Figures 4 and 5, respectively. The BBGFL results are in good agreement with MoM.
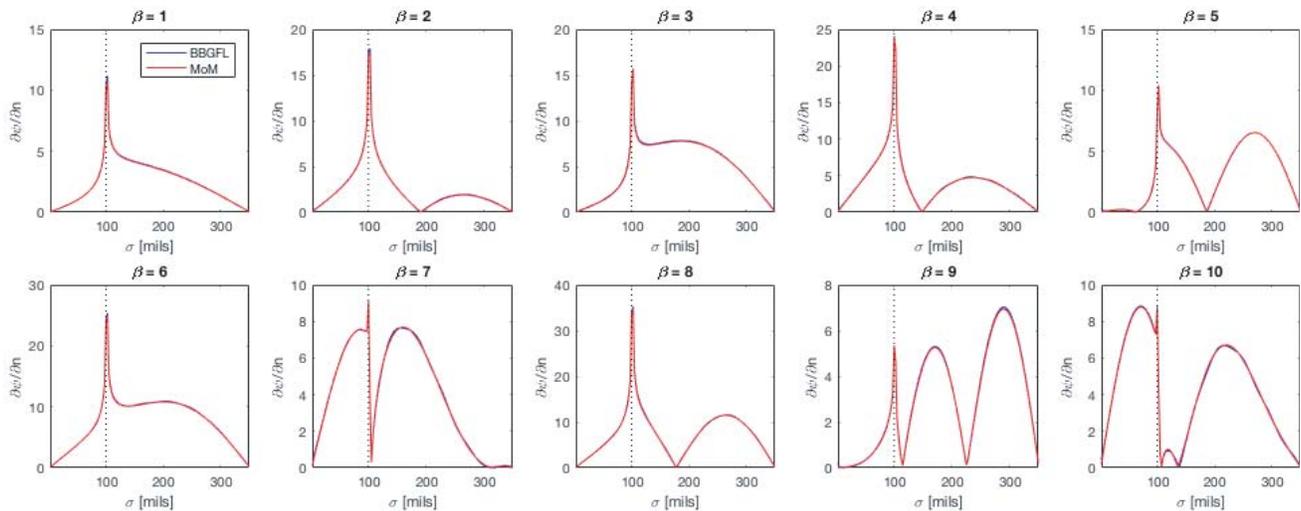
Figure 3. First 10 modal surface current of $\bar{z}_\beta$ on σ. (dot line for the corner).
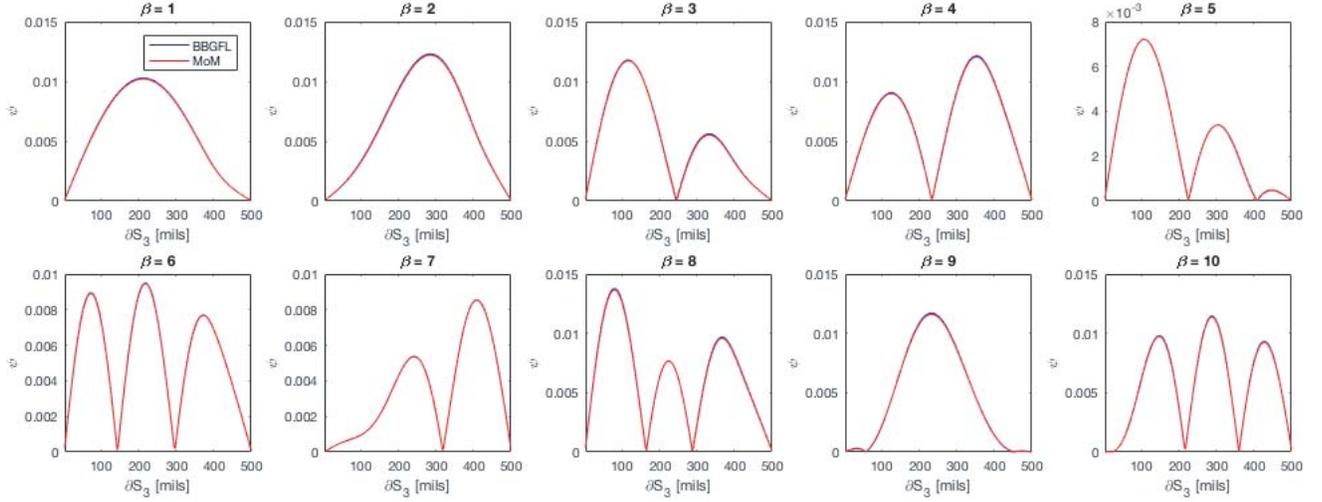
Figure 4. First 10 modal surface current of $\bar{x}_\beta$ on ∂S_3 (dielectric interface).
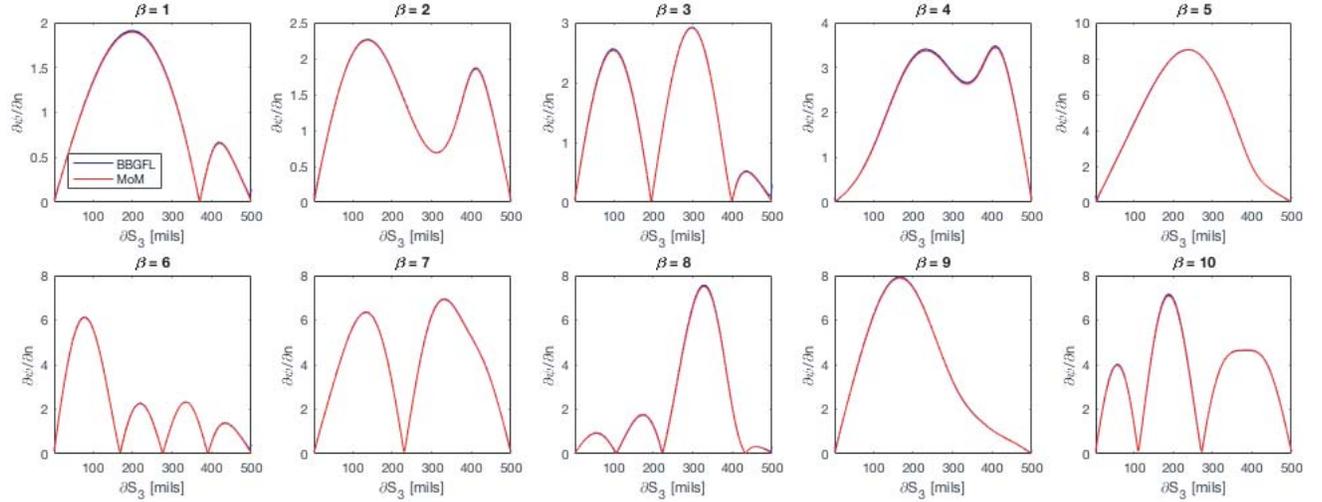
Figure 5. First 10 modal surface current of $\bar{y}_\beta$ on ∂S_3 (dielectric interface).

4.2. Spatial Responses of Green's Functions

The Green's function g_{11}^S are computed using Eqs. (53), (55), and (85) corresponding to the 2nd, 4th, and 6th order convergence, respectively. Similarly, Eqs. (54), (56), and (86) are for g_{21}^S. Let the source point be at $(30, 20)$ mils in A_1. The low wavenumbers are chosen to be $k_{1L}^S = 10$ and $k_{2L}^S = 7.14$ corresponding to frequency $f_L^S = 22.72$ MHz.

In Figure 6, we show the Green's function of waveguide S at 20 GHz along a vertical line at $x = -50$ mils. The dotted line denotes the location of dielectric interface ∂S_3. The results of g_{11}^S are on the right hand side of the dotted line, while g_{21}^S are on the left side. With 7 modal functions used in the modal summations, the 6th order results show the best agreement with MoM.

In Figure 7, the Green's function of waveguide S is plotted along a vertical line cross the source location. The 6th order BBGFL results are the closest to MoM results. The inset figure shows the good agreement between the 6th order BBGFL and MoM solutions near the source point. It clearly indicates that the usual modal summation of 2nd order has poor convergence when the observation point is close to the source point. The singular field behavior near the source location cannot be captured using finite number of modes in the second order modal representation. On the other hand, the low wavenumber
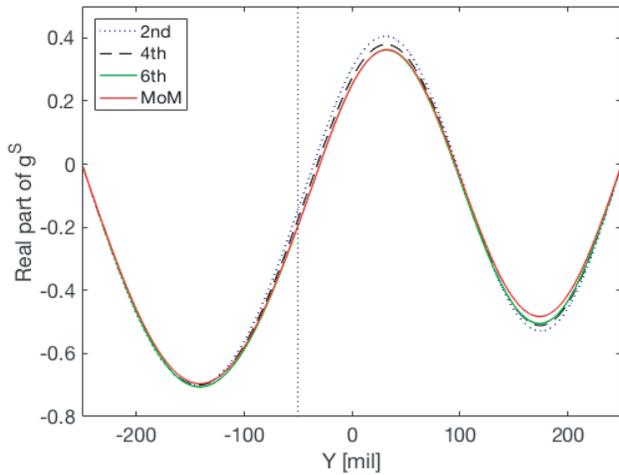
Figure 6. A vertical cut at $x = -50$ mils for Green's functions comparison with the target frequency of 20 GHz. 7 modal functions are applied for modal summations in 2nd, 4th, and 6th.
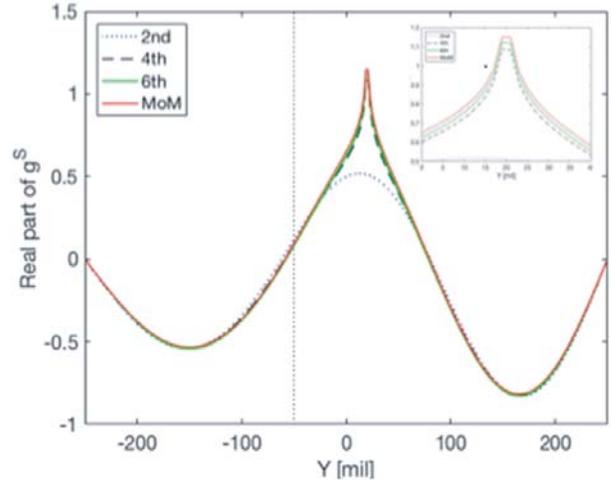
Figure 7. A vertical cut at $x = 30$ mils for Green's functions comparison with the target frequency of 20 GHz. 7 modal functions are applied for modal summations in 2nd, 4th, and 6th.

parts included in the 4th order and 6th order BBGFL results account for the low wavenumber solutions of MoM. The hybrid representations give good agreement with a relatively few numbers of modes.

In Figure 8 we show the contributions of low wavenumber terms, $g_{11}^S(k_{1L}^S, \bar{\rho}, \bar{\rho}'')$ and $g_{21}^S(k_{2L}^S, \bar{\rho}, \bar{\rho}'')$, wavenumber derivative terms, $[k_1^2 - (k_{1L}^S)^2][\frac{\partial g_{11}^S(k_1, \bar{\rho}, \bar{\rho}'')}{\partial k_1^2}]_{k_1=k_{1L}^S}$ and $[k_2^2 - (k_{2L}^S)^2][\frac{\partial g_{21}^S(k_2, \bar{\rho}, \bar{\rho}'')}{\partial k_2^2}]_{k_2=k_{2L}^S}$, and modal summation on the right hand side of Eqs. (85) and (86) to the BBGFL Green's function of 6th order. Near the source point, a peak is observed for the low wavenumber term. The other two terms are smooth over the source. The low wavenumber parts included in the 4th order and 6th order BBGFL expressions capture the singularity of waveguide Green's function.
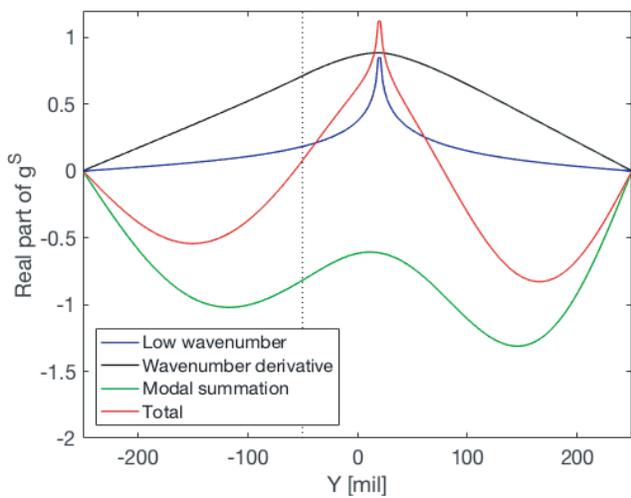
Figure 8. A vertical cut at $x = 30$ mils for the Green's function decomposition of 6th order. 7 modal functions are applied to modal summation at 20 GHz.
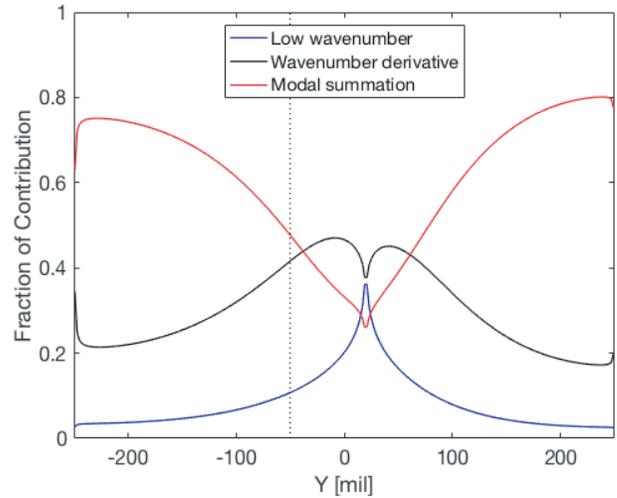
Figure 9. A vertical cut at $x = 30$ mils for the fraction contribution in Green's function of 6th order. 7 modal functions are applied to modal summation at 20 GHz.

A decomposition of BBGFL of 6th order is defined in Eq. (113).

$$C_{term}^{6th} = \frac{\left|g_{\xi1}^{S,term}\right|}{\left|g_{\xi1}^{S,Low}\right| + \left|g_{\xi1}^{S,Der}\right| + \left|g_{\xi1}^{S,Mod}\right|} \tag{113}$$

where $\xi = 1, 2$. In Figure 9, we compare the fractional contributions of low wavenumber, wavenumber derivative, and modal summation terms. Both the low wavenumber and wavenumber derivative terms show high contributions near the source than those of the modal summation. This shows that the higher order extraction improves the convergence around the source location. Since the low wavenumber is very low, the low wavenumber term contributions are significant near the source but decrease with distance away from the source. In Figure 10, we compare the contribution of individual mode to the 2nd, 4th, and 6th order BBGFLs at 20 GHz. The waveguide modes with frequencies higher than the operating frequency are evanescent modes. Others are propagation modes. The figure shows that the 6th order BBGFL have the least contributions from evanescent modes. The use of low wavenumber extraction in BBGFL reduces the need of higher order modes.
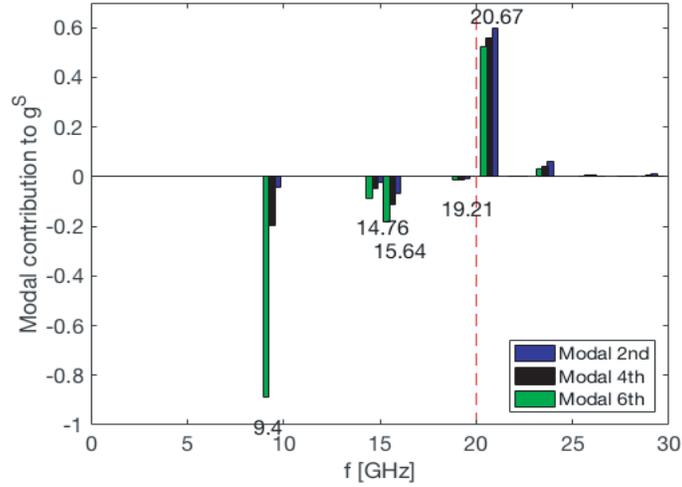
Figure 10. Individual contribution of β mode within modal summation. The target frequency is 20 GHz (dash line).

A significant feature of BBGFL is that the higher order BBGFL requires less number of modes in modal summation. We use MoM as reference and define the error.

$$error_{BBGFL}(\beta) = \frac{\left|g_{11}^{S,BBGFL}(\beta) - g_{11}^{S,MoM}\right|}{\left|g_{11}^{S,MoM}\right|} \tag{114}$$

Figure 11 shows the comparison of convergence with respect to the number of modes among 2nd, 4th, and 6th order BBGFLs for a single observation point close to the source. The 6th order BBGFL has 10 modes and the error is 2%. The error of 4th order BBGFL is about 5%. The 2nd order BBGFL has poor convergence around the source.

4.3. Broadband Response

BBGFL is efficient for broadband simulations, particularly in situations with multiple resonances. The broadband responses are shown in Figure 12. The results of BBGFLs (2nd, 4th, and 6th order) using 7 modes in modal summations are compared with those of MoM. The results of BBGFL are in good agreement with MoM. For frequencies approaching 20 GHz, the results start to deviate from MoM. With the same number of modal functions, the 6th order BBGFL gives the best agreement with MoM.
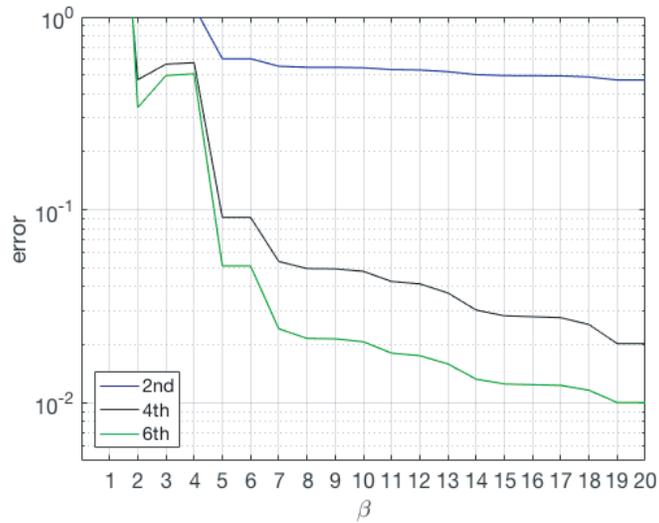
Figure 11. Convergence test w.r.t. number of β modes for a single point close to the source at 20 GHz. MoM is applied as reference.
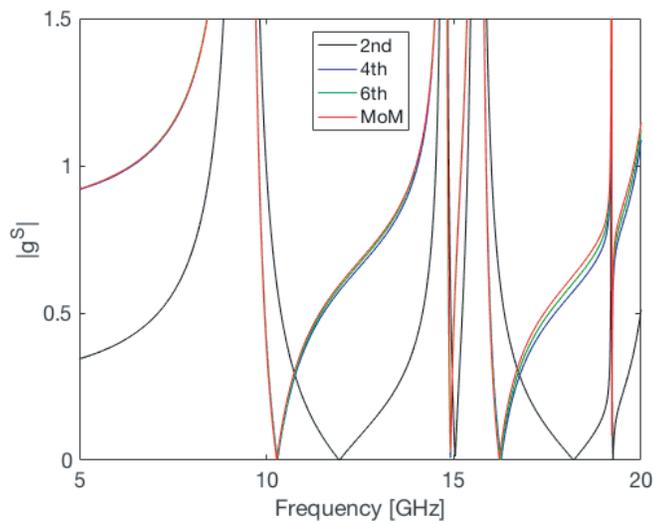
Figure 12. Frequency response of Green's functions for a single point close to the source. 7 modal functions are applied to modal summation.

Table 2. Simulation time.

	BBGFL, 6th order	MoM
Find resonant modes and apply normalization	30.78 (sec)	$2000 * 2.209 = 4418$ (sec)
Spurious modes rejection	6.61 (sec)	
Low wavenumber extraction & Wavenumber derivative	3.03 (sec)	
Broadband computation	$2000 * 0.00186 = 3.72$ (sec)	
Total	44.14 (sec)	

Table 2 shows the CPU for the 6th order BBGFL and MoM. BBGFL has a one-time overhead including (i) calculations of modal functions and resonance frequencies, (ii) normalization, (iii) rejection of spurious modes, and (iv) low wavenumber extraction and wavenumber derivative. The bulk overhead falls on finding resonant modes. Improving CPU time is our ongoing study. For 2000 frequency points, the 6th order BBGFL shows 100 times faster than MoM. The computations were performed using Intel Core i5@1.8 GHz with 8 GB memory.

5. CONCLUSIONS

The BBGFL method has been applied to the inhomogeneous waveguide of the TM case to calculate broadband Green's functions. Low wavenumber extractions of two g^Ω are used to form linear eigenvalue equation. To construct Green's function g^S, a single low frequency is applied to low wavenumber extraction and wavenumber derivative of currents and Green's functions. Results are in good agreement with the results of direct MoM. The 6th order BBGFL has less contribution from evanescent modes in modal summation, thus reducing the need of computing higher order modes.

Classically Green's function of waveguide only exists for separable geometry such as circular waveguide and rectangular waveguide. For inhomogeneous waveguide, Green's functions only exist for concentric circular layering. The merit of BBGFL is that it has widened the domain of Green's function to cover inhomogeneous waveguides and waveguides of irregular shape. An attractive merit of BBGFL is the broadband nature of the solutions since the results with varying frequencies are accomplished by merely changing the denominator. We are studying the extensions to the 3D case. Similar methodology has been used in periodic structures [17, 18, 20]. Recently there are works on Green's functions of resonant nano-structures [21] at close to resonant frequencies and piecewise homogeneous lossy waveguide [22].

REFERENCES

1. Tai, C. T., *Dyadic Green Functions in Electromagnetic Theory*, IEEE Press, 1994.
2. Collin, R. E., *Field Theory of Guided Waves*, IEEE Press, 1991.
3. Chew, W. C., *Waves and Fields in Inhomogeneous Media*, IEEE Press, 1995.
4. Tsang, L., J. A. Kong, and K. H. Ding, *Scattering of Electromagnetic Waves, Vol. 1: Theory and Applications*, Wiley Interscience, 2000.
5. Tsang, L., J. A. Kong, K. H. Ding, and C. Ao, *Scattering of Electromagnetic Waves*, Vol. 2, Wiley, New York, NY, USA, 2001.
6. Conciauro, G., M. Guglielmi, and R. Sorrentino, *Advanced Modal Analysis: CAD Techniques for Waveguide Components and Filters*, Wiley, NY, USA, 2002.
7. Bozzi, M., L. Perregrini, and K. Wu, "Modeling of conductor, dielectric, and radiation losses in substrate integrated waveguide by the boundary integral-resonant mode expansion method," *IEEE Trans. Microw. Theory Tech.*, Vol. 56, No. 12, 3153–3161, Dec. 2008.
8. Arcioni, P., M. Bozzi, M. Bressan, G. Conciauro, and L. Perregrini, "The BI-RME method: An historical overview," *2014 International Conference on Numerical Electromagnetic Modeling and Optimization for RF, Microwave, and Terahertz Applications (NEMO)*, May 14–16, 2014.
9. Tsang, L. and S. Huang, "Broadband Green's function with low wavenumber extraction for arbitrary shaped waveguide and applications to modeling of vias in finite power/ground plane," *Progress In Electromagnetic Research*, Vol. 152, 105–125, 2015.
10. Tsang, L. and S. Huang, "Full wave modeling and simulations of the waveguide behavior of printed circuit boards using a broadband Green's function technique," U.S. Patent 62/152 702, Apr. 24, 2015.
11. Huang, S., "Broadband Green's function and applications to fast electromagnetic analysis of high-speed interconnects," Ph.D. dissertation, Dept. Elect. Eng., Univ. Washington, Seattle, WA, USA, Jun. 2015.

12. Huang, S. and L. Tsang, "Fast electromagnetic analysis of emissions from printed circuit board using broadband Green's function method," *IEEE Trans. on Electromagnetic Compatibility*, Vol. 58, 1642–1652, 2016.

13. Huang, S. and L. Tsang, "Fast broadband modelling of traces connecting vias in printed circuit boards using broadband Green's function method," *IEEE Transactions on Components, Packaging and Manufacturing Technology*, Vol. 7, No. 8, 1343–1355, Aug. 2017.

14. Liao, T.-H., K.-H. Ding, and L. Tsang, "High order extractions of broadband Green's Function with low wavenumber extractions for arbitrary shaped waveguide," *Progress In Electromagnetic Research*, Vol. 158, 7–20, 2017.

15. Tsang, L., K.-H. Ding, T.-H. Liao, and S. Huang, "Modeling of scattering in arbitrary-shape waveguide using broadband Green's function with higher order low wavenumber extractions," *IEEE Trans. on Electromagnetic Compatibility*, Vol. 60, 16–25, 2018.

16. Tsang, L., "Broadband calculations of band diagrams in periodic structures using the broadband Green's function with low wavenumber extraction (BBGFL)," *Progress In Electromagnetics Research*, Vol. 153, 57–68, 2015.

17. Tsang, L. and S. Tan, "Calculations of band diagrams and low frequency dispersion relations of 2D periodic dielectric scattering using broadband Green's function with low wavenumber extraction (BBGFL)," *Optics Express*, Vol. 24, No. 2, 945–965, 2016.

18. Tan, S. and L. Tsang, "Green functions, including scatterers, for photonic crystals and metamaterials," *Journal of Optical Society of America B*, Vol. 34, 1450–1458, 2017.

19. Tsang, L., K.-H. Ding, and S. Tan, "Broadband point source Green's function in a one-dimensional infinite periodic lossless medium based on BBGFL with modal method," *Progress In Electromagnetic Research*, Vol. 163, 57–77, 2018.

20. Tan, S., "Multiple volume scattering in random media and periodic structures with applications in microwave remote sensing and wave functional materials," Ph.D. thesis, University of Michigan, 2016.

21. Chen, P. Y., D. J. Bergman, and Y. Sivan, "Rigorous expansion of electromagnetic Green's tensor of lossy resonators in open systems," *Proc. SPIE 10346, Plasmonics: Design, Materials, Fabrication, Characterization, and Applications XV*, 103460P, Aug. 25, 2017.

22. Bressan, M., S. Battistutta, M. Bozzi, and L. Perregrini, "Modeling of inhomogeneous and lossy waveguide components by the segmentation technique combined with the calculation of Green's function by Ewald's method," *IEEE Transactions on Microwave Theory and Techniques*, Vol. 66, 633–642, 2018.